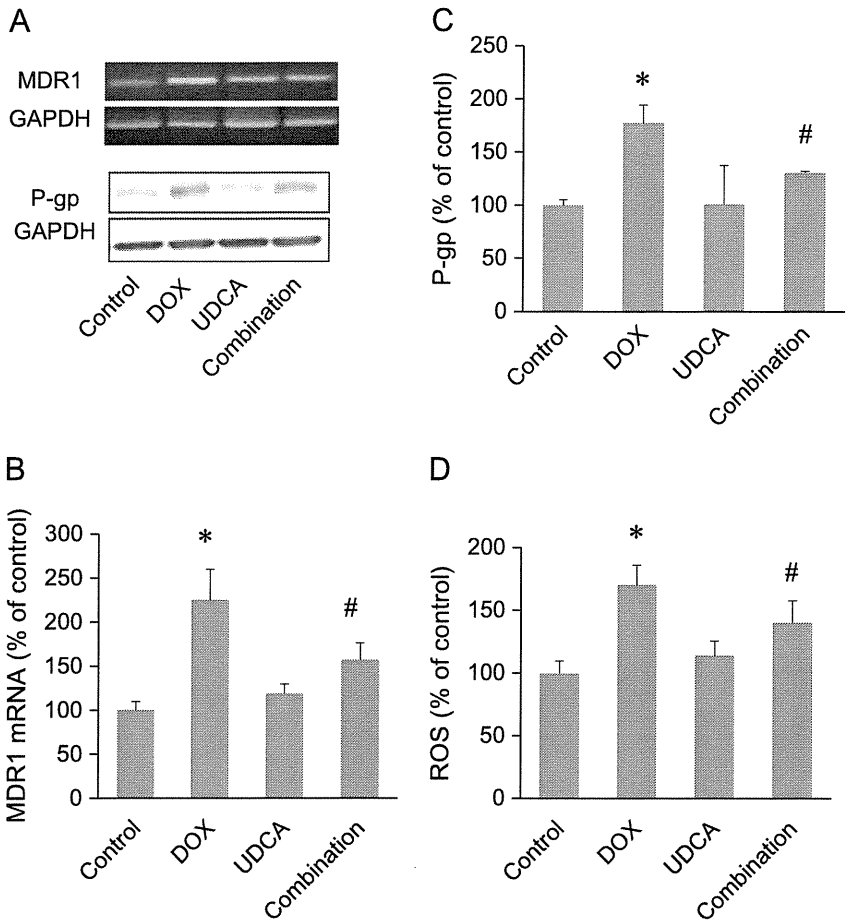

Fig. 3. Inhibitory effects of UDCA on the DOX-induced elevation in MDR1 mRNA, P-gp, and reactive oxygen species levels in HepG2 cells. HepG2 cells were pre-incubated with or without 100 μM UDCA, and were then cultivated with 3 μM DOX in the presence or absence of 100 μM UDCA for 24 h. RT-PCR (A, B), western blot analysis (A, C), and the determination of intracellular reactive oxygen species levels (D) were then conducted. Total RNA was extracted from the cells, and RT-PCR analysis of MDR1 mRNA and GAPDH mRNA was conducted (A, B). Whole cell lysates were used for western blot analysis of P-gp and GAPDH (A, C). Intracellular reactive oxygen species levels were determined using the fluorogenic dye CDCFH (D). The photograph is typical of three independent experiments. Column graph data represent relative levels against GAPDH and are expressed as the mean ± S.D. ($n=3$). $^{*}P<0.05$, significantly different from the control. $^{\#}P<0.05$, significantly different from the DOX group.

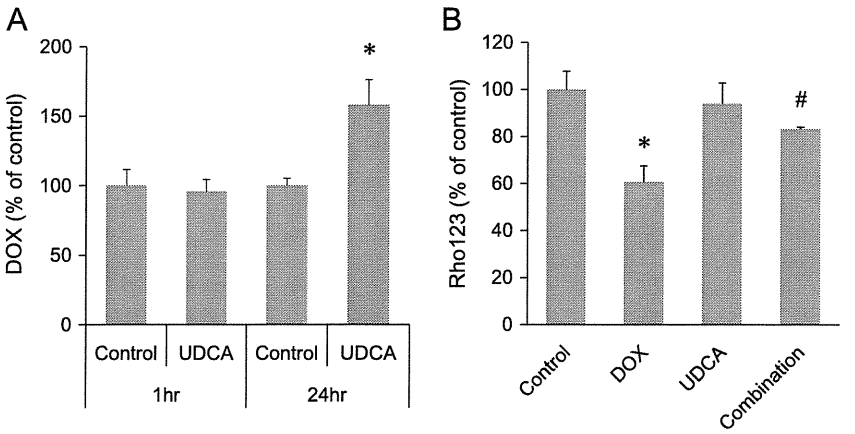

Fig. 4. Effects of UDCA on the intracellular accumulation of DOX and Rho123 in HepG2 cells. (A) HepG2 cells were pre-incubated with or without 100 μM UDCA for 1 h and then incubated with 3 μM DOX in the presence or absence of 100 μM UDCA for 1 or 24 h. Intracellular DOX levels were determined as described in the Materials and methods. (B) Cells were pre-incubated with or without 100 μM of UDCA for 1 h and then incubated with 3 μM DOX in the presence or absence of UDCA for 24 h. After changing to fresh medium, the cells were subsequently cultivated for 24 h. Cells were then incubated in fresh medium containing 3 μM Rho123 for 30 min at 37 °C. Intracellular Rho123 levels were determined as described in the Materials and methods. Fluorescence intensities of DOX and Rho123 are expressed as a relative value against cellular protein. Column graph data are expressed as the mean ± S.D. ($n=3$). $^{*}P<0.05$, significantly 1 different from the control. $^{\#}P<0.05$, significantly different from the DOX group.

DOX was previously shown to induce both an increase in intracellular reactive oxygen species content and decrease in GSH content accompanied by the activation of NF-κB (Ortiz et al., 2008). In the present study, we showed that UDCA and CDCA suppressed DOX-induced reactive oxygen species production, accompanied by the overexpression of MDR1 and P-gp, whereas DCA and LCA did not. Furthermore, we ascertained that NAC, an antioxidant, suppressed DOX-induced reactive oxygen

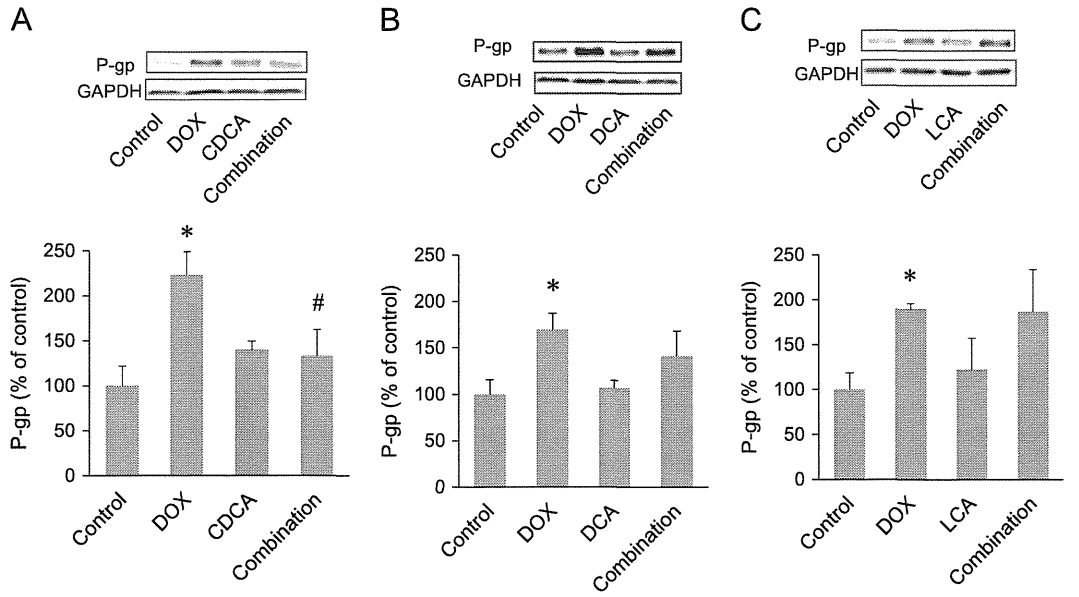

Fig. 5. Effect of CDCA, DCA, and LCA on the DOX-induced increase in P-gp levels. HepG2 cells were pre-incubated with or without 100 μM CDCA (A), 100 μM DCA (B), or 30 μM LCA (C) for 1 h and then incubated with 3 μM DOX in the presence or absence of a bile acid for 24 h. Whole cell lysates were used for western blot analysis. The photograph is typical of three independent experiments. Column graph data represent relative levels against GAPDH and are expressed as the mean ± S.D. ($n=3$). $^{*}P<0.05$, significantly different from the control. $^{\#}P<0.05$, significantly different from the DOX group.

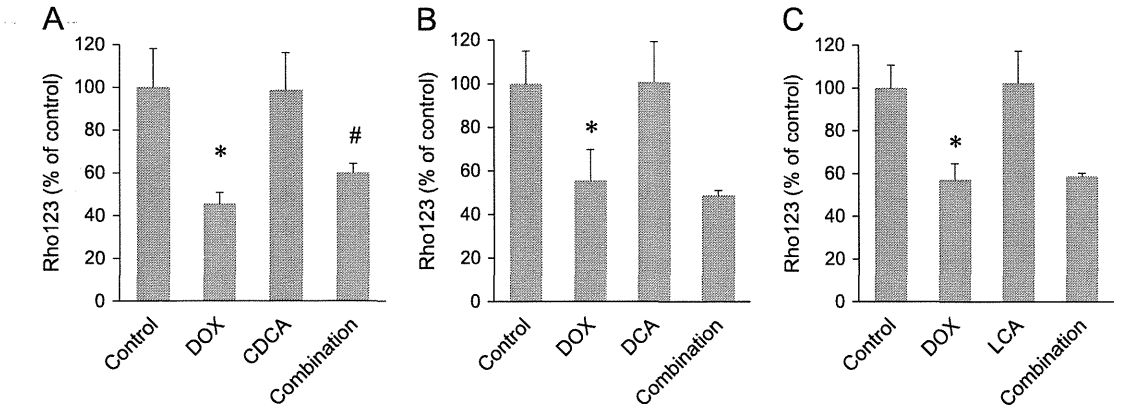

Fig. 6. Effects of CDCA, DCA, and LCA on the uptake of Rho123 in cells. HepG2 cells were pre-incubated with or without 100 μM CDCA (A), 100 μM DCA (B), or 30 μM LCA (C) for 1 h and then incubated with 3 μM DOX in the presence or absence of a bile acid for 24 h. After the cells were further cultivated in fresh medium for 24 h, they were incubated in fresh medium containing 3 μM Rho123 for 30 min at 37 °C. Fluorescence intensity was evaluated as a relative value against intracellular protein. Column graph data are expressed as the mean ± S.D. ($n=3$–6). $^{*}P<0.05$, significantly different from the control. $^{\#}P<0.05$, significantly different from the DOX group.

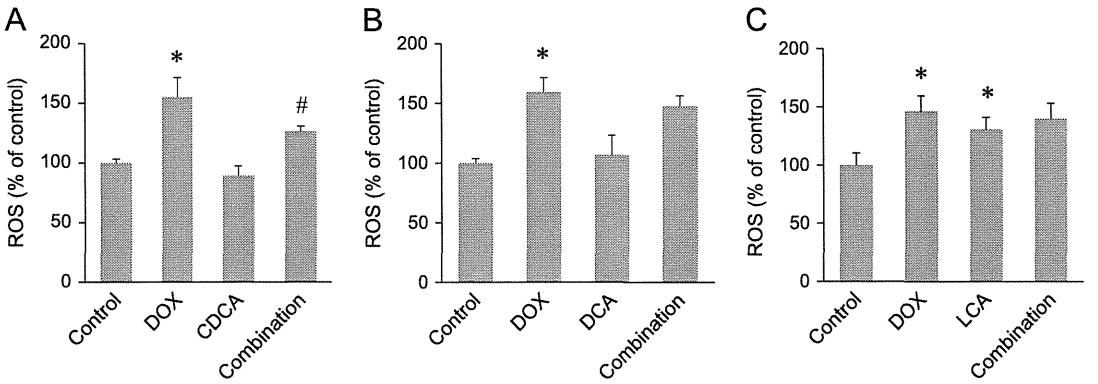

Fig. 7. Effects of CDCA, DCA, and LCA on reactive oxygen species levels in cells. After the pre-incubation of HepG2 cells with or without 100 μM CDCA (A), 100 μM DCA (B), or 30 μM LCA (C), cells were incubated with or without 3 μM DOX for 3 h in the presence or absence of bile acids. Intracellular reactive oxygen species levels were determined using the fluorogenic dye CDCFH. Fluorescence intensity was evaluated as a relative value against intracellular protein. Column graph data are expressed as the mean ± S.D. ($n=3$). $^{*}P<0.05$, significantly different from the control. $^{\#}P<0.05$, significantly different from the DOX group.

species production and the overexpression of MDR1mRNA in HepG2 cells. These results suggested that UDCA and CDCA inhibited the up-regulation of P-gp by eliminating DOX-induced reactive oxygen species and down-regulating cell signaling mediated by reactive oxygen species. The promoter region in the MDR1 gene has been shown to contain several elements responsive to NF-κB, SP-1, and PXR (Labialle et al., 2002; Bentires-Alj et al., 2003; Cornwell and Smith, 1993; Hu et al., 2000; Kurose et al., 2005). Although their exact role has not yet been clarified, reactive oxygen species has been shown to activate NF-κB signaling (Sen and Packer, 1996). On the other hand, it has been indicated that cadmium induced up-regulation of the MDR1 gene by activating NF-κB, and that this up-regulation was inhibited by antioxidants, NAC and pyrrolidine dithiocarbamate, suggesting that up-regulation of the MDR1 gene by cadmium may be mediated by reactive oxygen species and NF-κB signaling (Thévenod et al., 2000). These findings suggest that the DOX-induced overexpression of MDR1 mRNA and P-gp may be dependent on DOX-induced reactive oxygen species production and subsequent activation of NF-κB cell signaling and that UDCA inhibits these DOX-induced effects.

In this study, UDCA and CDCA inhibited the DOX-induced up-regulation of P-gp and UDCA reversed the decreased uptake of Rho123. Thus, UDCA exerted a marked effect on membrane transport function in DOX-treated HepG2 cells. CDCA has been shown to induce reactive oxygen species production and apoptosis in cells (Chu et al., 2003; Barrasa et al., 2011; Rosignoli et al., 2008). Indeed, our preliminary data indicated that 100 μM of CDCA slightly increased reactive oxygen species levels after incubation for 24 h, while UDCA did not up-regulate reactive oxygen species levels in HepG2 cells (data not shown). UDCA is well-known to be relatively hydrophilic and less cytotoxic than CDCA and the secondary bile acids. Considering these findings, the pre- and co-administration of UDCA should have the beneficial effect of regulating P-gp overexpression and preventing the acquisition of antitumor multidrug resistance in hepatocellular carcinoma treated with DOX or other anthracycline antitumor agents.

5. Conclusions

UDCA inhibited the DOX-induced overexpression of P-gp and restored the DOX-induced reduction in the accumulation of Rho123, accompanied by the suppression of DOX-induced increases in reactive oxygen species levels. The pre- and co-administration of UDCA may be helpful in preventing the acquisition of multidrug resistance to DOX for the treatment of hepatocellular carcinoma.

References

Arisawa, S., Ishida, K., Kameyama, N., Ueyama, J., Hattori, A., Tatsumi, Y., Hayashi, H., Yano, M., Hayashi, K., Katano, Y., Goto, H., Takagi, K., Wakusawa, S., 2009. Ursodeoxycholic acid induces glutathione synthesis through activation of PI3K/Akt pathway in HepG2 cells. Biochem. Pharmacol. 77, 858–866.

Barrasa, J.I., Olmo, N., Pérez-Ramos, P., Santiago-Gómez, A., Lecona, E., Turnay, J., Lizarbe, M.A., 2011. Deoxycholic and chenodeoxycholic bile acids induce apoptosis via oxidative stress in human colon adenocarcinoma cells. Apoptosis 16, 1054–1067.

Bates, D.A., Winterbourn, C.C., 1982. Deoxyribose breakdown by the adriamycin semiquinone and H_2O_2: evidence for hydroxyl radical participation. FEBS Lett. 145, 137–142.

Becquemont, L., Glaeser, H., Drescher, S., Hitzl, M., Simon, N., Murdter, T.E., Heinkele, G., Hofmann, U., Schaefer, C., Burk, O., Verstuyft, C., Eichelbaum, M., Fromm, M.F., 2006. Effects of ursodeoxycholic acid on P-glycoprotein and cytochrome P450 3A4-dependent pharmacokinetics in humans. Clin. Pharmacol. Ther. 79, 449–460.

Bentires-Alj, M., Barbu, V., Fillet, M., Chariot, A., Relic, B., Jacobs, N., Gielen, J., Merville, M.P., Bours, V., 2003. NF-kappaB transcription factor induces drug resistance through MDR1 expression in cancer cells. Oncogene 22, 90–97.

Borst, P., Elferink, R.O., 2002. Mammalian ABC transporters in health and disease. Annu. Rev. Biochem. 71, 537–592.

Chu, S.H., Lee-Kang, J., Lee, K.H., Lee, K., 2003. Roles of reactive oxygen species, NF-kappaB, and peroxiredoxins in glycochenodeoxycholic acid-induced rat hepatocytes death. Pharmacology 69, 12–19.

Cornwell, M.M., Smith, D.E., 1993. SP1 activates the MDR1 promoter through one of two distinct G-rich regions that modulate promoter activity. J. Biol. Chem. 268, 19505–19511.

Corpechot, C., Carrat, F., Bonnand, A.M., Poupon, R.E., Poupon, R., 2000. The effect of ursodeoxycholic acid therapy on liver fibrosis progression in primary biliary cirrhosis. Hepatology 32, 1196–1199.

Cotter, M.A., Thomas, J., Cassidy, P., Robinette, K., Jenkins, N., Florell, S.R., Leachman, S., Samlowski, W.E., Grossman, D., 2007. N-acetylcysteine protects melanocytes against oxidative stress/damage and delays onset of ultraviolet-induced melanoma in mice. Clin. Cancer Res. 13, 5952–5958.

Dussault, I., Yoo, H.D., Lin, M., Wang, E., Fan, M., Batta, A.K., Salen, G., Erickson, S.K., Forman, B.M., 2003. Identification of an endogenous ligand that activates pregnane X receptor-mediated sterol clearance. Proc. Natl. Acad. Sci. USA 100, 833–838.

Geick, A., Eichelbaum, M., Burk, O., 2001. Nuclear receptor response elements mediate induction of intestinal MDR1 by rifampin. J. Biol. Chem. 276, 14581–14587.

Hu, X.F., Slater, A., Wall, D.M., Kantharidis, P., Parkin, J.D., Cowman, A., Zalcberg, J.R., 1995. Rapid up-regulation of mdr1 expression by anthracyclines in a classical multidrug-resistant cell line. Br. J. Cancer 71, 931–936.

Hu, Z., Jin, S., Scotto, K.W., 2000. Transcriptional activation of the MDR1 gene by UV irradiation. Role of NF-Y and Sp1. J. Biol. Chem. 275, 2979–2985.

Jemal, A., Bray, F., Center, M.M., Ferlay, J., Ward, E., F 1 Orman, D., 2011. Global cancer statistics. CA Cancer J. Clin. 61, 69-90. Erratum in. CA Cancer J. Clin. 61, 134.

Kanda, Y., 2013. Investigation of the freely available easy-to-use software 'EZR' for medical statistics. Bone Marrow Transpl. 48, 452–458.

Kawata, K., Kobayashi, Y., Souda, K., Kawamura, K., Sumiyoshi, S., Takahashi, Y., Noritake, H., Watanabe, S., Suehiro, T., Nakamura, H., 2010. Enhanced hepatic Nrf2 activation after ursodeoxycholic acid treatment in patients with primary biliary cirrhosis. Antioxid. Redox Signal. 13, 259–268.

Kneuer, C., Honscha, W., Gäbel, G., Honscha, K.U., 2007. Adaptive response to increased bile acids: induction of MDR1 gene expression and P-glycoprotein activity in renal epithelial cells. Pflugers Arch. 454, 587–594.

Kurose, K., Koyano, S., Ikeda, S., Tohkin, M., Hasegawa, R., Sawada, J., 2005. 5′ diversity of human hepatic PXR (NR1I2) transcripts and identification of the major transcription initiation site. Mol. Cell. Biochem. 273, 79–85.

Labialle, S., Gayet, L., Marthinet, E., Rigal, D., Baggetto, L.G., 2002. Transcriptional regulators of the human multidrug resistance 1 gene: recent views. Biochem. Pharmacol. 264, 943–948.

Mitsuyoshi, H., Nakashima, T., Sumida, Y., Yoh, T., Nakajima, Y., Ishikawa, H., Inaba, K., Sakamoto, Y., Okanoue, T., Kashima, K., 1999. Ursodeoxycholic acid protects hepatocytes against oxidative injury via induction of antioxidants. Biochem. Biophys. Res. Commun. 263, 537–542.

Myers, C.E., McGuire, W.P., Liss, R.H., Ifrim, I., Grotzinger T, K., Young, R.C., 1977. Adriamycin: the role of lipid peroxidation in cardiac toxicity and tumor response. Science 197, 165–167.

Okada, K., Shoda, J., Taguchi, K., Maher, J.M., Ishizaki, K., Inoue, Y., Ohtsuki, M., Goto, N., Takeda, K., Utsunomiya, H., Oda, K., Warabi, E., Ishii, T., Osaka, K., Hyodo, I., Yamamoto, M., 2008. Ursodeoxycholic acid stimulates Nrf2-mediated hepatocellular transport, detoxification and antioxidative stress systems in mice. Am. J. Physiol. Gastrointest. Liver Physiol. 295, G735–G747.

Omata, M., Yoshida, H., Toyota, J., Tomita, E., Nishiguchi, S., Hayashi, N., Iino, S., Makino, I., Okita, K., Toda, G., Tanikawa, K., Kumada, H., 2007. A large-scale, multicentre, double-blind trial of ursodeoxycholic acid in patients with chronic hepatitis C. Gut 56, 1747–1753.

Ortiz, C., Caja, L., Sancho, P., Bertran, E., Fabregat, I., 2008. Inhibition of the EGF receptor blocks autocrine growth and increases the cytotoxic effects of doxorubicin in rat hepatoma cells: role of reactive oxygen species production and glutathione depletion. Biochem. Pharmacol. 75, 1935–1945.

Rajesh, K.G., Suzuki, R., Maeda, H., Yamamoto, M., Yutong, X., Sasaguri, S., 2005. Hydrophilic bile salt ursodeoxycholic acid protects myocardium against reperfusion injury in a PI3K/Akt dependent pathway. J. Mol. Cell. Cardiol. 39, 766–776.

Rosignoli, P., Fabiani, R., De Bartolomeo, A., Fuccelli, R., Pelli, M.A., Morozzi, G., 2008. Genotoxic effect of bile acids on human normal and tumour colon cells and protection by dietary antioxidants and butyrate. Eur. J. Nutr. 47, 301–309.

Sen, C.K., Packer, L., 1996. Antioxidant and redox regulation of gene transcription. Faseb J. 10, 709–720.

Thévenod, F., Friedmann, J.M., Katsen, A.D., Hauser, I.A., 2000. Up-regulation of multidrug resistance P-glycoprotein via nuclear factor-kappaB activation protects kidney proximal tubule cells from cadmium- and reactive oxygen species-induced apoptosis. J. Biol. Chem. 275, 1887–1896.

Tinkle, C.L., Haas-Kogan, D., 2012. Hepatocellular carcinoma: natural history, current management, and emerging tools. Biologics 6, 207–219.

Ziemann, C., Bürkle, A., Kahl, G.F., Hirsch-Ernst, K.I., 1999. Reactive oxygen species participate in mdr1b mRNA and P-glycoprotein overexpression in primary rat hepatocyte cultures. Carcinogenesis 20, 407–414.

Sphingosine-1-phosphate-mediated osteoclast precursor monocyte migration is a critical point of control in antibone-resorptive action of active vitamin D

Junichi Kikuta[a,b], Shunsuke Kawamura[a,b], Fumie Okiji[a,b], Mai Shirazaki[a,b], Sadaoki Sakai[c], Hitoshi Saito[c], and Masaru Ishii[a,b,1]

[a]Laboratory of Cellular Dynamics, Immunology Frontier Research Center, Osaka University, Osaka 565-0871, Japan; [b]Japan Science and Technology, Core Research for Evolutionary Science and Technology, Tokyo 102-0075, Japan; and [c]Medical Affairs Division, Chugai Pharmaceutical Co., Ltd., Tokyo 103-8324, Japan

Edited by Hector F. DeLuca, University of Wisconsin, Madison, WI, and approved March 12, 2013 (received for review October 30, 2012)

The migration and positioning of osteoclast precursor monocytes are controlled by the blood-enriched lipid mediator sphingosine-1-phosphate (S1P) and have recently been shown to be critical points of control in osteoclastogenesis and bone homeostasis. Here, we show that calcitriol, which is the hormonally active form of vitamin D, and its therapeutically used analog, eldecalcitol, inhibit bone resorption by modulating this mechanism. Vitamin D analogs have been used clinically for treating osteoporosis, although the mode of its pharmacologic action remains to be fully elucidated. In this study, we found that active vitamin D reduced the expression of S1PR2, a chemorepulsive receptor for blood S1P, on circulating osteoclast precursor monocytes both in vitro and in vivo. Calcitriol- or eldecalcitol-treated monocytoid RAW264.7 cells, which display osteoclast precursor-like properties, migrated readily to S1P. Concordantly, the mobility of circulating CX_3CR1^+ osteoclast precursor monocytes was significantly increased on systemic administration of active vitamin D. These results show a mechanism for active vitamin D in controlling the migratory behavior of circulating osteoclast precursors, and this action should be conducive to limiting osteoclastic bone resorption in vivo.

chemotaxis | imaging | treatment | immunology | circulation

Bone is a highly dynamic organ, and it is continuously remodeled cooperatively by bone-resorbing osteoclasts and bone-replenishing osteoblasts (1). Osteoclasts, which have bone-resorbing capacity, are a unique cell type differentiated from monocyte/macrophage lineage hematopoietic precursor cells termed osteoclast precursors. Previous studies have identified key molecular signals, such as mediated by macrophage colony-stimulating factor (M-CSF) and receptor activator of NF-κB ligand (RANKL), that regulate osteoclastic differentiation and function (2, 3). Unlike osteoblasts, which are of mesenchymal origin and essentially reside in bone tissues, osteoclasts and their precursor monocytes are highly dynamic. Their migratory mechanisms in systemic circulation and homing into bone spaces have recently emerged as critical points of control for osteoclastogenesis and thus, bone homeostasis. We have recently used intravital two-photon microscopy to visualize the bone tissues of live mice and found that sphingosine-1-phosphate (S1P), a lysophospholipid mediator enriched in blood, plays a vital role in regulating the migration and positioning of osteoclast precursors on the bone surface (4, 5).

Osteoclast precursor monocytes express S1PR1 (formerly designated as $S1P_1$ or Edg-1), a cognate receptor for S1P, and can use this receptor to migrate from bone tissues to blood that contains S1P. The deletion of S1PR1 in monocytoid cells leads to an accumulation of osteoclast precursors and a resultant increase in bone resorption, which suggests that the S1P–S1PR1 interaction is essential for the recirculation of osteoclast precursors from bone to blood (4). The expression of S1PR1 was suppressed on stimulation with RANKL, representing a reasonable mechanism where monocytoid precursors, after initiating a commitment to osteoclast differentiation, can no longer recirculate into the blood.

Successive studies have shown that osteoclast precursors also express S1PR2 ($S1P_2$ or Edg-5), another cognate receptor that negatively regulates S1P (4, 6). Although S1PR1 exerts positive chemotaxis to an S1P gradient, S1PR2 inhibits the positive chemotaxis induced by S1PR1 or induces migration in the inverse direction along the S1P gradient—so-called chemorepulsion (7). The deletion of S1PR2 led to moderate osteopetrosis attributable to a decrease in osteoclast recruitment onto the bone surface, indicating that S1PR2-mediated chemorepulsion against blood S1P contributes to the homing of osteoclast precursors into bone spaces (6). Most studies have shown that the migration of osteoclast precursors is reciprocally regulated by two counteracting receptors, circulation-attractive S1PR1 and bone-tropic S1PR2, and that their entrance into and exit from the bones are finely tuned by these accelerators and brakes. More importantly, it was shown that either activation of S1PR1 or blockade of S1PR2 could relieve bone density loss in a murine osteoporosis model by inhibiting bone homing of osteoclast precursor monocytes (4, 6). These results have garnered great attention regarding drug discovery. Many of the antibone-resorptive agents developed thus far, including bisphosphonate (8) and cathepsin K inhibitors (9, 10), target fully matured osteoclasts, whereas treatments targeting monocytoid early osteoclast precursors, such as S1P modulators, would provide a unique line of therapy for bone loss. Here, we reveal that an antibone-resorptive drug with this type of pharmacologic profile already exists—the vitamin D hormone.

Vitamin D was first identified as an antirachitic factor and has been clinically shown to improve calcium balance in both young and elderly populations. Active vitamin D analogs have been used clinically in several countries for treating bone and mineral disorders associated with chronic kidney diseases or osteoporosis, although their direct pharmacologic mechanisms in bone are not fully understood (11, 12). Notably, active vitamin D metabolites, such as calcitriol [$1\alpha,25(OH)_2D_3$ (1,25-D)], have been shown to increase the expression of RANKL in bone marrow stromal cells, thereby acting as osteoclastogenic, bone-resorbing factors (13, 14). These findings have raised an intractable paradox regarding the action on bone of vitamin D (15–17).

In the present study, we first show that the active form of vitamin D, 1,25-D, and its clinically used analog, eldecalcitol (ELD), significantly suppress the expression of bone-tropic S1PR2 in

Author contributions: M.I. designed research; J.K., S.K., F.O., M.S., and H.S. performed research; S.S. and H.S. contributed new reagents/analytic tools; and J.K. and M.I. wrote the paper.

Conflict of interest statement: S.S. and H.S. are full-time employees of Chugai Pharmaceutical Co., Ltd. All other authors have no conflicts of interest.

This article is a PNAS Direct Submission.

Freely available online through the PNAS open access option.

[1]To whom correspondence should be addressed. E-mail: mishii@ifrec.osaka-u.ac.jp.

This article contains supporting information online at www.pnas.org/lookup/suppl/doi:10.1073/1218799110/-/DCSupplemental.

circulating osteoclast precursor monocytes and block osteoclastic bone resorption by mobilizing precursor monocytes from the bone to the blood. This study shows that the control of osteoclast precursor monocyte migration is a target of the antibone-resorptive action of vitamin D.

Results

Active Vitamin D, 1,25-D, and Its Therapeutically Used Analog, ELD, Suppress the Expression of S1PR2 in Circulating Osteoclast Precursor Monocytes. To investigate the potential role of vitamin D signaling in the control of osteoclast precursor monocyte mobilization, we examined the effects of the active form of vitamin D, 1,25-D, and its clinically used active vitamin D analog, ELD, on the expression of several chemokine receptors in a monocytoid cell line, RAW264.7, which because it can be differentiated into giant osteoclast-like cells on stimulation with RANKL, is considered to be a cell line with osteoclast precursor-like capacity (18). Both 1,25-D and ELD significantly suppressed the expression of S1PR2 in a dose-dependent manner (Fig. 1*A*), whereas the expression levels of other chemokine receptors, including S1PR1, CXCR4, and CX_3CR1, were essentially unaltered (Fig. S1). This down-regulation of S1PR2 was observed only in RAW264.7 cells that were cultured under floating conditions; these cells tend to undergo transformation into macrophage-like cells when grown in adherent cultures (Fig. S2*A*), which leads to reduced expression of the vitamin D receptor (VDR) (Fig. S2*B*) and loss of responsiveness to VDR stimulation (Fig. S2*C*). These results suggest that this regulation of expression is critically dependent on VDR in these cell types.

S1P-mediated chemotaxis of osteoclast precursor monocytes was previously shown to be reciprocally regulated by two counteracting cognate receptors, S1PR1 and S1PR2 (4, 6). S1PR1 is a major high-affinity receptor that induces positive migration along an S1P concentration gradient, whereas S1PR2 has a lower affinity and inhibits S1PR1-mediated chemotaxis and/or induces migration in an inverse direction (chemorepulsion). At lower doses of S1P (10^{-8} M), osteoclast precursor monocytes readily moved to the S1P gradient. Their movement was abolished at higher doses of S1P (10^{-6} M), because the negative receptor S1PR2 was activated. Concordant with previously obtained results, the RAW264.7 cells hardly moved in 10^{-6} M S1P under the control condition (Fig. 1 *B*, *Left* and *C*). Conversely, the cells that were preincubated with 1,25-D (Fig. 1 *B*, *Center* and *C*) or ELD (Fig. 1 *B*, *Right* and *C*) migrated to the higher concentration (10^{-6} M) of S1P; a similar finding was reported for S1PR2-knockdown RAW264.7 cells (6). These results clearly show that 1,25-D– or ELD-induced down-regulation of S1PR2 leads to enhanced migration to a high concentration of S1P, such as found in the blood (19).

Although the definition of osteoclast precursors remains controversial, monocytoid cells that express colony stimulating factor 1 receptor (CSF1R)/c-Fms are thought to contain precursor cells that can differentiate into osteoclasts (20). In addition, CX_3CR1, which is a cognate receptor for CX_3CL1/fractalkine that is preferentially expressed in monocytoid cell types, is considered a good marker of osteoclast precursors (6, 21, 22). We sorted CSF1R- or CX_3CR1-positive cells from CSF1R-EGFP transgenic (20) or CX_3CR1-EGFP knockin (21) mice, respectively, and treated the sorted cells with ELD (10^{-9} to 10^{-8} M) in floating cultures. The expression levels of S1PR2 in both cell types were significantly and dose-dependently suppressed by VDR stimulation (Fig. S3). The decrease in S1PR2 expression was more prominent in these cases compared with the decrease in expression observed in floating RAW264.7 cells.

1,25-D and ELD Ameliorate Ovariectomy-Induced Bone Density Loss and Suppress the Expression of S1PR2 in Circulating Monocytoid Osteoclast Precursors in Vivo. Next, we examined the effects on mice of in vivo treatment with 1,25-D and ELD. According to the previously reported protocol, 1,25-D or ELD (dosage of 50 ng/kg body weight for each) dissolved in a vehicle [medium chain triglyceride (MCT)] was orally administered to the mice for 4 wk. Concordant with the previous data (23, 24), oral treatment with 1,25-D or ELD prevented ovariectomy-induced bone loss and significantly recovered the bone mineral densities compared with vehicle control (Fig. 2 *A* and *B*). Under this condition, we examined the expression of S1PR2 in $CD11b^+$-circulating monocytes, including osteoclast precursors. The $CD11b^+$ cells in mice that were treated orally with 1,25-D or ELD expressed lower levels of S1PR2 than cells that were subjected to the control conditions (Fig. 2*C*). These results suggest that oral administration of active vitamin D, or analogs thereof, suppresses S1PR2 expression in osteoclast precursor monocytes in vivo.

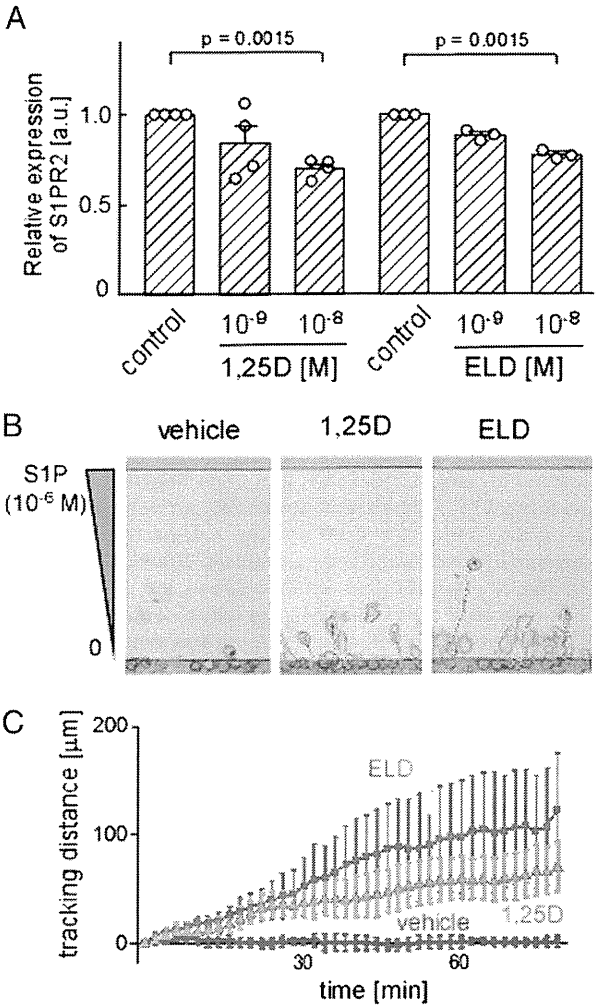

Fig. 1. Suppression of S1PR2 expression and gain of chemotactic activity to S1P in RAW264.7 osteoclast precursors after treatment with 1,25-D or ELD. (*A*) Quantitative real-time PCR analysis of S1PR2 mRNA expressed by RAW264.7 cells in floating cultures. Both 1,25-D and ELD suppress the expression of S1PR2 in a dose-dependent manner in floating cultures. Error bars represent ± SEM ($n = 3$ for each). (*B*) In vitro S1P-directed chemotaxis of RAW264.7 cells pretreated with vehicle (*Left*) (Movie S1), 1,25-D (*Center*) (Movie S2), or ELD (*Right*) (Movie S3) and dynamically visualized using EZ-Taxiscan. The cells are loaded into the lower chamber. The upper chamber is filled with medium that contains 10^{-6} M S1P. Cells migrate into the terrace between the loading chambers. The height from the bottom to the top of the terrace is 8 μm. (Scale bar: 100 μm.) (*C*) Migration distances derived from microscopy analyses of RAW264.7 cells pretreated with vehicle (red), 1,25-D (green), or ELD (blue). The experiments were independently performed three times, and the data are largely consistent. Each dot represents the mean value of 10 independent cells, and error bars represent ± SEM.

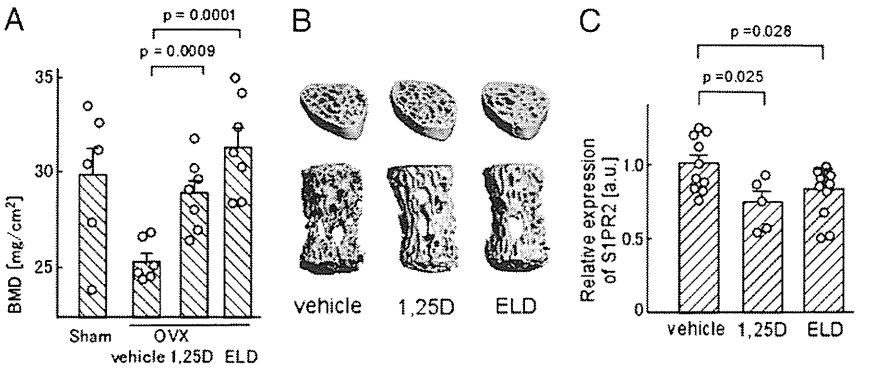

Fig. 2. In vivo impacts of 1,25-D and ELD on bone remodeling. (*A*) Preventive effects of 1,25-D and ELD on ovariectomy-induced osteoporosis. Lumbar vertebrae were collected from mice that were sham-operated; ovariectomized and vehicle-treated; ovariectomized and 1,25-D–treated; and ovariectomized and ELD-treated. Bone mineral density was measured by dual-energy X-ray absorptiometry. Error bars represent ± SEM (n = 6 or 7 for each). (*B*) Micro-computed tomography images of lumbar vertebrae from ovariectomized mice treated with vehicle (*Left*), 1,25-D (*Center*), and ELD (*Right*). (*C*) Quantitative real-time PCR analysis of S1PR2 mRNA expressed by $CD11b^+$ cells sorted from WT mice that were treated orally with vehicle only, 1,25-D, or ELD daily for 5 d. Error bars represent ± SEM (n = 10 for vehicle-treated; n = 5 for 1,25-D–treated; n =10 for ELD-treated).

Finally, we examined the in vivo mobility of CX_3CR1-$EGFP^+$ osteoclast precursor monocytes in living bone tissues using intravital multiphoton bone microscopy according to methods that we originally established (4, 6). CX_3CR1-EGFP knockin mice were treated orally with 1,25-D or ELD (50 ng/kg body weight) or vehicle (MCT) for 5 d, and the bone tissues of the mice were visualized to assess the mobilities of the $EGFP^+$ cells (Fig. 3). The mobility of the CX_3CR1-$EGFP^+$ monocytoid cells was significantly increased in mice that were treated with ELD, which is similar to what was observed after treatment with an S1PR2 antagonist (6). These results clearly show that in vivo oral treatment with 1,25-D or ELD suppresses S1PR2 expression and the mobilization of osteoclast precursor monocytes from the bone to the blood circulation, thereby contributing to limiting osteoclastic bone destruction, which is the main therapeutic effect of active vitamin D drugs.

Discussion

Active vitamin D analogs have been used for treating bone and mineral disorders, mainly osteoporosis. The precise pharmacologic action has remained elusive, although previous reports have indicated that c-fos, an osteoclastogenic transcription factor (23), and RANKL expression in osteoblasts (24) may be the targets of vitamin D action. In the present study, we reveal a point of control by active vitamin D: the control of osteoclast precursor monocyte migration. Because this therapeutic point is independent of the points exploited by conventional antibone-resorptive drugs, such as bisphosphonate, it may provide a unique avenue of treatment for bone diseases. Currently, combination therapy with active vitamin D and bisphosphonate is the most effective treatment (25–27), which suggests synergistic therapeutic effects of bisphosphonate and vitamin D acting at respectively different therapeutic points.

ELD has been screened for its high therapeutic potency in treating bone diseases (28–30). However, because its pharmacologic profile, which includes binding affinity for VDR, is similar to the profiles of the active form of vitamin D, 1,25-D, and other active vitamin D analogs, such as alfacalcidol, the mechanism underlying its superior therapeutic effect is currently unknown (29, 31). One characteristic of ELD is its high binding affinity for vitamin D binding protein in serum (32), suggesting that ELD is more readily maintained in the blood. This point of action of vitamin D would be particularly advantageous in relation to its actions on circulating osteoclast precursor monocytes.

Recently, we reported that a high concentration of S1P in blood is critically maintained by an S1P transporter, spns2, which is expressed in vascular endothelial cells (33). Genetic ablation of spns2 in mice led to an almost 50% decrease in blood S1P, and the migration rates of T and B lymphocytes, which express S1P receptors, were greatly impaired (33). Moreover, in these

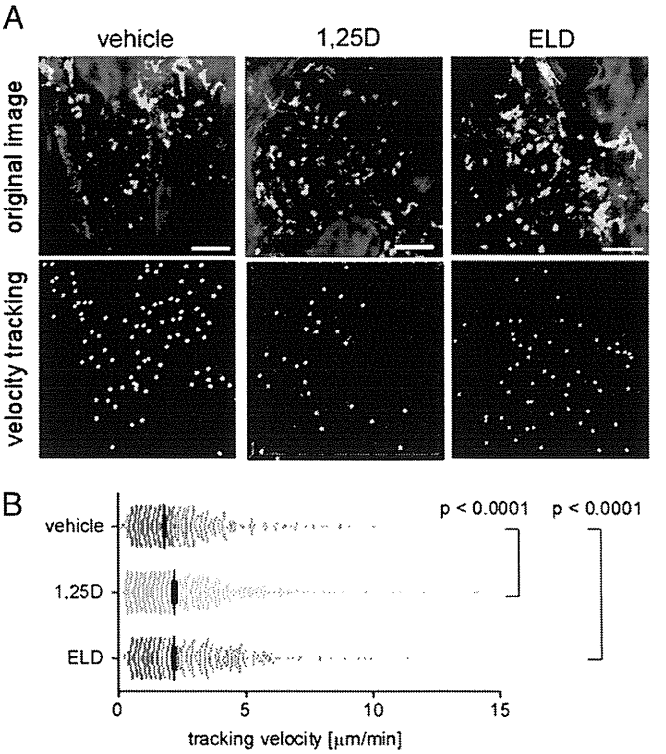

Fig. 3. In vivo S1PR2-mediated control of migration of osteoclast precursor monocytes visualized using intravital multiphoton imaging. (*A*) Intravital multiphoton imaging of the skull bone tissues of heterozygous CX_3CR1-EGFP knockin mice that were treated orally with vehicle only (*Left*) (Movie S4), 1,25-D (*Center*) (Movie S5), or ELD (*Right*) (Movie S6) daily for 5 d. CX_3CR1-EGFP–positive cells appear green. The microvasculature was visualized by i.v. injection of Texas Red-conjugated 70 kDa dextran (red). The blue color indicates the bone surface (*Upper*). The movements of the CX_3CR1-EGFP–positive cells were tracked for 20 min. Colored lines show the associated trajectories of the cells (*Lower*). (Scale bars: 50 μm.) (*B*) Summary of the mean tracking velocities of CX_3CR1-EGFP–positive cells treated with vehicle (red circles), 1,25-D (green circles), and ELD (blue circles). Data points (n = 708 for vehicle-treated; n = 507 for 1,25-D–treated; n = 520 for ELD-treated) represent the values for individual cells compiled from six independent experiments, and error bars represent ± SEM.

mice, the bone mineral density was largely changed, suggesting the significance of S1P for physiologic bone metabolism. More importantly, a recent clinical investigation has shown that the serum concentration of S1P is critically correlated with bone mineral density and the incidence of bone fractures in humans (34). These lines of in vivo evidence in mice and humans strongly support our notion that ELD, which is stably present in circulating blood, could be beneficial for suppressing S1PR2 in circulating monocytes and blocking osteoclastogenesis and bone resorption.

Vitamin D is a multifunctional hormone that is essential for humans. Vitamin D has been reported to play crucial roles not only in the endocrine system and metabolism but also, in immunity (35), cancer biology (36), and neuroscience (37), although the pharmacologic actions have not been fully clarified in most cases. S1P and its cognate receptors, such as S1PR2, are also multifunctional and have been shown to be involved in immune regulation by controlling the chemotactic activities of various immune cells (38, 39). Now that active vitamin D has been shown to control the S1P system in bone metabolism, the actions of vitamin D related to S1P signaling should be examined in various other biological systems. These analyses may contribute to additional development of active vitamin D analogs for the treatment of several human diseases in addition to bone diseases.

Materials and Methods

Mice. C57BL/6 mice were obtained from CREA Japan. CSF1R (M-CSF receptor) -EGFP transgenic mice (20) and CX_3CR1-EGFP knockin mice (21) were obtained from Jackson Laboratory. All mice were bred and maintained under specific pathogen-free conditions at the animal facilities of Osaka University (Osaka, Japan), and all animal experiments were performed according to institutional animal experimental guidelines under approved protocols from the Animal Experimental Committee of Osaka University.

Cell Culture. RAW264.7, which is a mouse macrophage/monocyte lineage cell line, was cultured with or without 1,25-D or ELD (Chugai Pharmaceuticals Co., Ltd.) for 2 d using a low-cell binding dish (Nalge Nunc), the surface of which was coated with 2-methacryloxyethyl phosphorylcholine. After incubation, total RNA was extracted from the cells, and quantitative real-time PCR was performed. Bone marrow cells were isolated from CSF1R-EGFP transgenic or CX_3CR1-EGFP knockin mice, and the EGFP-positive cells were sorted using the FACS Aria flow cytometer (BD Biosciences). The cells were cultured in a low-cell binding dish with 25 ng/mL M-CSF (PeproTech) for 5 d; 1,25-D or ELD was added to the medium, and the cells were incubated for an additional 2 d. After incubation, total RNA was extracted from the cells, and quantitative real-time PCR was performed.

Quantitative real-time PCR. Quantitative teal-time PCR was performed using the Thermal Cycler Dice Real-Time System TP800 (Takara) and the following specific primer pairs (forward and reverse, respectively): S1PR2 (5′-CCAAGGAGACGCTGGACATG-3′ and 5′-TGCCGTAGAGCTTGACCTTGTCGAA-3′); VDR (5′-AACGCTATGACCTGTGAAGGC-3′ and 5′-CCTGTACTTACGTCTGCACGA-3′); and GAPDH (5′-ACCACAGTCCATGCCATCAC-3′ and 5′-TCCACCACCCTGTTGCTGTA-3′).

EZ-Taxiscan Chemotaxis Assay. Chemotaxis experiments were conducted in an EZ-Taxiscan chamber according to the manufacturer's protocol (GE Healthcare). The EZ-Taxiscan is a visually accessible chemotactic chamber, in which one compartment that contains the ligand (S1P) and another compartment that contains the cells are connected by a microchannel. A stable concentration gradient of chemoattractant can be reproducibly formed and maintained through the channel without medium flow. Phase-contrast images of migrating cells were acquired at 1-min intervals. Sequential image data were processed using the ImageJ program (National Institutes of Health) with an add-on program, MT Track J.

Ovariectomy and Bone Histomorphometry. Nine-week-old female C57BL/6J mice, which were ovariectomized or sham-operated, were injected orally with 1,25-D (50 ng/kg body weight) dissolved in vehicle (MCT; Nisshin Oillio), ELD (50 ng/kg body weight) in vehicle, or vehicle only daily for 4 wk. At the end of the treatment period, the mice were euthanized, and the lumbar vertebrae were excised and fixed in 70% (vol/vol) ethanol. The uteri of all of the animals were excised and weighed to evaluate the effect of ovariectomy. Bone mineral density was measured by dual-energy X-ray absorptiometry (DCS-600EX; Aloka) at the second to fifth vertebrae. 3D trabecular analysis of the lumbar vertebral body was performed by microcomputed tomography (μCT 40; Scanco Medical).

1,25-D and ELD Treatment. C57BL6/J mice were treated orally with 1,25-D (50 ng/kg body weight) in vehicle, ELD (50 ng/kg body weight) in vehicle, or vehicle only daily for 5 d. In some experiments, the mice were then killed, and $CD11b^+$ cells were separated using autoMACS (Miltenyi Biotec) from the spleen and bone marrow, which contain a high number of circulating monocytoid cells. Total RNA was extracted from the cells, and quantitative real-time PCR was performed.

Multiphoton Intravital Bone Tissue Imaging. Intravital microscopy of mouse calvaria bone tissues was performed using a protocol modified from a previous study (4); 10- to 14-wk-old mice were anesthetized using isoflurane [Escain; 2.0% (vol/vol) vaporized in 100% (vol/vol) oxygen], the frontoparietal region of the skull bone was exposed, and the internal surfaces of bones adjacent to the bone marrow cavity were observed using multiphoton excitation microscopy. The imaging system was composed of a multiphoton microscope (A1-MP; Nikon) driven by a laser (Chameleon Vision II Ti: Sapphire; Coherent) tuned to 880 nm together with an upright microscope equipped with a 25× water immersion objective (APO, N.A. 1.1; Nikon). Fluorescent cells were detected through bandpass emission filters at 500/50 nm (for EGFP). Vessels were visualized by intravenously injecting Texas Red-conjugated 70 kDa dextran (detected using a 601/56-nm filter) immediately before imaging. Image stacks were collected at a 5-μm vertical step size at a depth of 100–150 μm below the skull bone surface. Raw imaging data were processed using Imaris (Bitplane) with a Gaussian filter for noise reduction. Automatic 3D object tracking with Imaris Spots was aided by manual corrections to retrieve cell spatial coordinates over time.

Statistical Analysis. The Mann–Whitney rank-sum test was used to calculate the *P* values for highly skewed distributions. For Gaussian-like distributions, two-tailed *t* tests were used.

ACKNOWLEDGMENTS. This study was supported by Grant-in-Aid 22689030 for Encouragement of Young Scientists (A; to M.I.), Grant-in-Aid 22113007 for Scientific Research on Innovative Areas (to M.I.), a Funding Program for World-Leading Innovative R&D on Science and Technology (FIRST Program) from the Ministry of Education, Science, Sports and Culture of Japan (to M.I.), and Grants CDA-00059/2009 and RGY0077/2011 from the International Human Frontier Science Program (to M.I.).

1. Teitelbaum SL (2000) Bone resorption by osteoclasts. *Science* 289(5484):1504–1508.
2. Teitelbaum SL, Ross FP (2003) Genetic regulation of osteoclast development and function. *Nat Rev Genet* 4(8):638–649.
3. Karsenty G, Wagner EF (2002) Reaching a genetic and molecular understanding of skeletal development. *Dev Cell* 2(4):389–406.
4. Ishii M, et al. (2009) Sphingosine-1-phosphate mobilizes osteoclast precursors and regulates bone homeostasis. *Nature* 458(7237):524–528.
5. Klauschen F, et al. (2009) Quantifying cellular interaction dynamics in 3D fluorescence microscopy data. *Nat Protoc* 4(9):1305–1311.
6. Ishii M, Kikuta J, Shimazu Y, Meier-Schellersheim M, Germain RN (2010) Chemorepulsion by blood S1P regulates osteoclast precursor mobilization and bone remodeling in vivo. *J Exp Med* 207(13):2793–2798.
7. Okamoto H, et al. (2000) Inhibitory regulation of Rac activation, membrane ruffling, and cell migration by the G protein-coupled sphingosine-1-phosphate receptor EDG5 but not EDG1 or EDG3. *Mol Cell Biol* 20(24):9247–9261.
8. Russell RG, et al. (2007) Bisphosphonates: An update on mechanisms of action and how these relate to clinical efficacy. *Ann N Y Acad Sci* 1117:209–257.
9. Bone HG, et al. (2010) Odanacatib, a cathepsin-K inhibitor for osteoporosis: A two-year study in postmenopausal women with low bone density. *J Bone Miner Res* 25(5):937–947.
10. Eisman JA, et al. (2011) Odanacatib in the treatment of postmenopausal women with low bone mineral density: Three-year continued therapy and resolution of effect. *J Bone Miner Res* 26(2):242–251.
11. Bouillon R, Okamura WH, Norman AW (1995) Structure-function relationships in the vitamin D endocrine system. *Endocr Rev* 16(2):200–257.
12. Plum LA, DeLuca HF (2010) Vitamin D, disease and therapeutic opportunities. *Nat Rev Drug Discov* 9(12):941–955.
13. Roodman GD, Ibbotson KJ, MacDonald BR, Kuehl TJ, Mundy GR (1985) 1,25-Dihydroxyvitamin D3 causes formation of multinucleated cells with several osteoclast characteristics in cultures of primate marrow. *Proc Natl Acad Sci USA* 82(23): 8213–8217.

14. Yasuda H, et al. (1998) Osteoclast differentiation factor is a ligand for osteoprotegerin/osteoclastogenesis-inhibitory factor and is identical to TRANCE/RANKL. *Proc Natl Acad Sci USA* 95(7):3597–3602.
15. Suda T, et al. (1999) Modulation of osteoclast differentiation and function by the new members of the tumor necrosis factor receptor and ligand families. *Endocr Rev* 20(3): 345–357.
16. Suda T, Ueno Y, Fujii K, Shinki T (2003) Vitamin D and bone. *J Cell Biochem* 88(2): 259–266.
17. Suda T, Takahashi F, Takahashi N (2012) Bone effects of vitamin D - Discrepancies between in vivo and in vitro studies. *Arch Biochem Biophys* 523(1):22–29.
18. Ishii M, et al. (2006) RANKL-induced expression of tetraspanin CD9 in lipid raft membrane microdomain is essential for cell fusion during osteoclastogenesis. *J Bone Miner Res* 21(6):965–976.
19. Maeda Y, Seki N, Sato N, Sugahara K, Chiba K (2010) Sphingosine 1-phosphate receptor type 1 regulates egress of mature T cells from mouse bone marrow. *Int Immunol* 22(6):515–525.
20. Burnett SH, et al. (2004) Conditional macrophage ablation in transgenic mice expressing a Fas-based suicide gene. *J Leukoc Biol* 75(4):612–623.
21. Jung S, et al. (2000) Analysis of fractalkine receptor CX(3)CR1 function by targeted deletion and green fluorescent protein reporter gene insertion. *Mol Cell Biol* 20(11): 4106–4114.
22. Koizumi K, et al. (2009) Role of CX3CL1/fractalkine in osteoclast differentiation and bone resorption. *J Immunol* 183(12):7825–7831.
23. Takasu H, et al. (2006) c-Fos protein as a target of anti-osteoclastogenic action of vitamin D, and synthesis of new analogs. *J Clin Invest* 116(2):528–535.
24. Harada S, et al. (2012) Daily administration of eldecalcitol (ED-71), an active vitamin D analog, increases bone mineral density by suppressing RANKL expression in mouse trabecular bone. *J Bone Miner Res* 27(2):461–473.
25. Sakai S, Endo K, Takeda S, Mihara M, Shiraishi A (2012) Combination therapy with eldecalcitol and alendronate has therapeutic advantages over monotherapy by improving bone strength. *Bone* 50(5):1054–1063.
26. Sugimoto M, Futaki N, Harada M, Kaku S (2013) Effects of combined treatment with eldecalcitol and alendronate on bone mass, mechanical properties, and bone histomorphometry in ovariectomized rats: A comparison with alfacalcidol and alendronate. *Bone* 52(1):181–188.
27. Ringe JD, Farahmand P, Schacht E, Rozehnal A (2007) Superiority of a combined treatment of Alendronate and Alfacalcidol compared to the combination of Alendronate and plain vitamin D or Alfacalcidol alone in established postmenopausal or male osteoporosis (AAC-Trial). *Rheumatol Int* 27(5):425–434.
28. Matsumoto T, et al. (2005) A new active vitamin D, ED-71, increases bone mass in osteoporotic patients under vitamin D supplementation: A randomized, double-blind, placebo-controlled clinical trial. *J Clin Endocrinol Metab* 90(9):5031–5036.
29. Sanford M, McCormack PL (2011) Eldecalcitol: A review of its use in the treatment of osteoporosis. *Drugs* 71(13):1755–1770.
30. Matsumoto T, et al. (2011) A new active vitamin D3 analog, eldecalcitol, prevents the risk of osteoporotic fractures—a randomized, active comparator, double-blind study. *Bone* 49(4):605–612.
31. Ito M, Nakamura T, Fukunaga M, Shiraki M, Matsumoto T (2011) Effect of eldecalcitol, an active vitamin D analog, on hip structure and biomechanical properties: 3D assessment by clinical CT. *Bone* 49(3):328–334.
32. Okano T, et al. (1991) A novel synthetic vitamin D3 analogue, 2-beta-(3-hydroxypropoxy)-calcitriol (ED-71): Its biological activities and pharmacological effects on calcium metabolism. *Contrib Nephrol* 91:116–122.
33. Fukuhara S, et al. (2012) The sphingosine-1-phosphate transporter Spns2 expressed on endothelial cells regulates lymphocyte trafficking in mice. *J Clin Invest* 122(4): 1416–1426.
34. Lee SH, et al. (2012) Higher circulating sphingosine 1-phosphate levels are associated with lower bone mineral density and higher bone resorption marker in humans. *J Clin Endocrinol Metab* 97(8):E1421–E1428.
35. Bouillon R, et al. (2008) Vitamin D and human health: Lessons from vitamin D receptor null mice. *Endocr Rev* 29(6):726–776.
36. Vuolo L, Di Somma C, Faggiano A, Colao A (2012) Vitamin D and cancer. *Front Endocrinol (Lausanne)* 3:58.
37. Garcion E, Wion-Barbot N, Montero-Menei CN, Berger F, Wion D (2002) New clues about vitamin D functions in the nervous system. *Trends Endocrinol Metab* 13(3): 100–105.
38. Rosen H, Goetzl EJ (2005) Sphingosine 1-phosphate and its receptors: An autocrine and paracrine network. *Nat Rev Immunol* 5(7):560–570.
39. Cyster JG (2005) Chemokines, sphingosine-1-phosphate, and cell migration in secondary lymphoid organs. *Annu Rev Immunol* 23:127–159.

Carcinogenesis vol.35 no.2 pp.272–281, 2014
doi:10.1093/carcin/bgt343
Advance Access publication October 15, 2013

Heat shock factor 1 accelerates hepatocellular carcinoma development by activating nuclear factor-κB/mitogen-activated protein kinase

Makoto Chuma*, Naoya Sakamoto, Akira Nakai[1], Shuhei Hige, Mitsuru Nakanishi, Mitsuteru Natsuizaka, Goki Suda, Takuya Sho, Kanako Hatanaka[2], Yoshihiro Matsuno[2], Hideki Yokoo[3], Toshiya Kamiyama[3], Akinobu Taketomi[3], Gen Fujii[4], Kosuke Tashiro[5], Yoko Hikiba[6], Mitsuaki Fujimoto[1], Masahiro Asaka and Shin Maeda[7]

Department of Gastroenterology and Hepatology, Hokkaido University, Kita 15, Nishi 7, Kita-ku, Sapporo 060-8638, Japan, [1]Department of Biochemistry and Molecular Biology, Yamaguchi University, Ube, Japan, [2]Department of Pathology and [3]Department of Gastroenterological Surgery I, Hokkaido University, Kita 15, Nishi 7, Kita-ku, Sapporo 060-8638, Japan, [4]Division of Cancer Prevention, National Cancer Center Research Institute, Tokyo, Japan, [5]Graduate School of Genetic Resources Technology, Kyushu University, Fukuoka, Japan, [6]Division of Gastroenterology, Institute for Adult Diseases, Asahi Life Foundation, Tokyo, Japan and [7]Department of Gastroenterology, Yokohama City University, Yokohama, Japan

*To whom correspondence should be addressed. Tel: +81 11-716-1611; Fax: +81 11-706-7867;
Email: mchuuma@med.hokudai.ac.jp

Heat shock factor 1 (HSF1), a major transactivator of stress responses, has been implicated in carcinogenesis in various organs. However, little is known about the biological functions of HSF1 in the development of hepatocellular carcinoma (HCC). To clarify the functional role of HSF1 in HCC, we established HSF1-knockdown (HSF1 KD) KYN2 HCC cells by stably expressing either small hairpin RNA (shRNA) against HSF1 (i.e. HSF1 KD) or control shRNA (HSF1 control). Tumorigenicity was significantly reduced in orthotopic mice with HSF1 KD cells compared with those with HSF1 control cells. Reduced tumorigenesis in HSF1 KD cells appeared attributable to increased apoptosis and decreased proliferation. Tumor necrosis factor-α-induced apoptosis was increased in HSF1 KD cells and HSF1$^{-/-}$ mouse hepatocytes compared with controls. Decreased expression of IκB kinase γ, a positive regulator of nuclear factor-κB, was also observed in HSF1 KD cells and HSF1$^{-/-}$ mouse hepatocytes. Furthermore, expression of bcl-2-associated athanogene domain 3 (BAG3) was dramatically reduced in HSF1 KD cells and HSF1$^{-/-}$ mouse hepatocytes. We also found that epidermal growth factor-stimulated mitogen-activated protein kinase signaling was impaired in HSF1 KD cells. Clinicopathological analysis demonstrated frequent overexpression of HSF1 in human HCCs. Significant correlations between HSF1 and BAG3 protein levels and prognosis were also observed. In summary, these results identify a mechanistic link between HSF1 and liver tumorigenesis and may provide as a potential molecular target for the development of anti-HCC therapies.

Introduction

Hepatocellular carcinoma (HCC) is one of the most common malignant tumors and the third leading cause of cancer death worldwide (1). Despite marked advances in diagnostic and therapeutic techniques, prognosis remains unsatisfactory for HCC patients (2,3). An understanding of HCC carcinogenesis at the molecular level is thus urgently needed in order to identify novel molecular targets for the development of more effective therapies.

Heat shock factor 1 (HSF1) is the main regulator of the heat shock response, which is involved in protecting cells and organisms from heat, ischemia, inflammation, oxidative stress and other noxious conditions (4,5). Under various forms of physiological stress, HSF1 drives the production of heat shock proteins (HSPs), such as HSP27, HSP70 and HSP90, which act as protein chaperones (5,6). The functions of HSF1 are not limited to increasing the expression of chaperones; HSF1 also modulates the expression of hundreds of genes other than chaperones that are critical for survival under an array of potentially lethal stressors (6–8). As a result, HSF1 influences fundamental cellular processes such as cell cycle control, protein translation, glucose metabolism and proliferation (7–12). In human tumors, constitutive expression of Hsp27, Hsp70 and Hsp90 at high levels predicts poor prognosis and resistance to therapy (13–15). These effects are often attributable to HSF1-dependent mechanisms (16). Thus, as a master regulator of cellular processes, the roles of HSF1 in carcinogenesis and tumor progression are now emerging. Several recent investigations using mouse models have suggested that HSF1 is involved in carcinogenesis (9,17). In clinical samples, HSF1 is often constitutively expressed at high levels in a variety of tumors, including breast cancer (7,18), pancreatic cancer (19), prostate carcinoma (20) and oral squamous cell carcinoma (21).

Hepatocarcinogenesis is a multistep process, in the majority of cases slowly developing within a well-defined etiology of viral infection and chronic alcohol abuse, leading to the chronic hepatitis and cirrhosis that are regarded as preneoplastic stages (22). A great number of factors, receptors and downstream elements of signaling cascades regulate proliferation and apoptosis. Dysregulation of the balance between cell proliferation and apoptosis thus plays a critical role in hepatocarcinogenesis (23,24). Two of the major pathways of cell proliferation and apoptosis are nuclear factor kappa B (NF-κB) signaling and mitogen-activated protein kinase (MAPK) signaling. NF-κB transcription factors are critical regulators of genes involved in inflammation and the suppression of apoptosis. NF-κB has been shown to be instrumental for tumor promotion in colitis-associated cancer and inflammation-associated liver cancer (25,26). Activation of the extracellular signal-regulated kinase (ERK)/MAPK pathway regulates many important cellular processes, such as proliferation, differentiation, angiogenesis, survival and cell adhesion (27). Importantly, the ERK/MAPK pathway is constitutively activated in HCC (28).

The present study investigated the biological influences of HSF1 in HCC cell proliferation and apoptosis involving the NF-κB and MAPK signal pathways. We found that HSF1 deficiency significantly diminished NF-κB and MAPK activation in primary hepatocytes and HCC cells, so HSF1 deficiency inhibited the development of HCC. Furthermore, clinicopathological analysis demonstrated a significant correlation between HSF1 protein level and prognosis. Our results suggest HSF1 as a promising molecular target for the development of anti-HCC therapeutics.

Abbreviations: BAG3, bcl-2-associated athanogene domain 3; EGFR, epidermal growth factor receptor; ERK, extracellular signal-regulated kinase; FACS, fluorescence-activated cell sorting; HCC, hepatocellular carcinoma; HSF1, heat shock factor 1; HSF1 KD, HSF1 knockdown; HSP, heat shock protein; IKKγ, IκB kinase gamma; LPS, lipopolysaccharide; MAPK, mitogen-activated protein kinase; MEK, mitogen-activated protein kinase kinase; mRNA, messenger RNA; NF-κB, nuclear factor kappa B; PCNA, proliferating cell nuclear antigen; SCID, severe combined immune-deficient mice; shRNA, small hairpin RNA; TNF-α, tumor necrosis factor alpha; TUNEL, terminal deoxynucleotidyl transferase-mediated deoxyuridine triphosphate nick-end labeling; WT, wild type.

Materials and methods

Cell cultures and reagents

Human HCC cell lines HepG2, PLC/PRF/5, HLE and HLF were obtained from the American Type Culture Collection. Huh7 was obtained from the Japanese Collection of Research Bioresources Cell Bank (Ibaraki, Japan). KIM-1 and KYN2 were kindly provided by Dr Hirohisa Yano (Department of Pathology, Kurume University, Kurume, Japan). Li7 was kindly provided by Dr Yae Kanai (Division of Molecular Pathology, National Cancer Center Research Institute,

Tokyo, Japan). HepG2, PLC/PRF/5, Huh7, HLE and HLF cells were maintained in Dulbecco's modified Eagle's medium containing 10% fetal bovine serum. KIM-1 and KYN2 was maintained in RPMI medium containing 10% fetal bovine serum.

Antibodies and chemicals

The antibodies used included: anti-HSF1, ERK1/2, phosphor-ERK1/2, MAPK kinase (MEK), phospho-MEK, phosphor- efficiently activated epidermal growth factor receptor (EGFR), cyclin D1, cdc2, CDK4, phospho-IκBα, IκB kinase gamma (IKKγ), IKKβ, caspase-3 and Bcl-X_L (Cell Signaling Biotechnology, Danvers, MA); anti-HSP90, HSP72, β-actin and proliferating cell nuclear antigen (PCNA) (Santa Cruz Biotechnology, Santa Cruz, CA); anti-EGFR (Millipore, Billerica, MA); anti-HSP70/HSP72 (Enzo Life science, NY); and anti-BAG3 (Abcam, Cambridge, UK).

Biochemical and immunohistochemical analyses

Protein lysates were prepared from tissues and cultured cells, separated by sodium dodecyl sulfate–polyacrylamide gel electrophoresis, transferred onto Immobilon membranes (Millipore) and analyzed by immunoblotting. Total cellular RNA was extracted using Trizol reagent (Invitrogen, Carlsbad, CA), then cDNA was synthesized using SuperScript II (Invitrogen), and expression of specific messenger RNAs (mRNAs) was quantified using real-time PCR and normalized against glyceraldehyde-3-phosphate dehydrogenase mRNA expression. Details of real-time PCR conditions and primer sequences are available in Supplementary Materials and methods, available at *Carcinogenesis* Online. Immunohistochemical staining was performed on formalin-fixed, paraffin-embedded tissue sections using immunoperoxidase methods, as described previously (15). For array analysis, we used the Human WG-6 BeadChip-kit (Illumina, San Diego, CA) in accordance with the instructions from the manufacturer (details are given in Supplementary Materials and methods, available at *Carcinogenesis* Online).

Establishment of HSF1-knockdown cells

A HSF1 small hairpin RNA (shRNA) plasmid and negative control plasmid were purchased from SABiosciences (QIAGEN, Valencia, CA). The shRNA sequences targeting HSF1 were from position 5′-CAGGTTGTTCATAGTCAGAAT-3′ as in the nucleotide sequence of HSF1. As a negative control, a shRNA was designed with the sequence 5′-GGAATCTCATTCGATGCATAC-3′. Transfection was achieved using Oligofectamine reagent (Invitrogen) according to the instructions from the manufacturer. To establish stable knockdown cell lines, shRNA plasmids were transfected into KYN2 cells and cultured in the presence of puromycin (Sigma–Aldrich, St Louis, MO).

Cell proliferation and bromodeoxyuridine assay

Cell proliferation in response to HSF1 silencing was determined by trypan blue exclusion assay. DNA synthesis was determined by bromodeoxyuridine assay according to the instructions from the manufacturer (Roche Diagnostics, Basel, Switzerland). The result was expressed as a percentage of the maximum absorbance at 450nm, based on three independent experiments. Cells were counted using a Coulter Counter (Beckman Coulter, Pasadena, CA).

Apoptosis assay

Assessment of apoptosis was performed by measuring the intensity of the sub-G_1 peak. For the sub-G_1 peak, HSF1 control KYN2 cells or HSF1-knockdown (HSF1 KD) KYN2 cells were tumor necrosis factor alpha (TNF-α) treatment for 24 h. Cells were treated with propidium iodide and then the sub-G_1 peak was analyzed with a fluorescence-activated cell sorting (FACS) flow cytometer (FACSCalibur; Becton Dickinson, San Jose, CA). Terminal deoxynucleotidyl transferase-mediated deoxyuridine triphosphate nick-end labeling (TUNEL) assay was performed in accordance with the manufacturer's instructions (ApopTag kit; Intergen, Burlington, MA).

Animals

HSF1-deficient ($HSF^{-/-}$) mice have been described previously (29). C57BL/6 wild-type (WT) mice were purchased from CLEA Japan (Tokyo, Japan) for use in the experiments, with primary hepatocytes isolated using a collagenase perfusion method as described in a previous report (26). For orthotopic implantation, C.B-17/Icr-scid/scidJcl [severe combined immune-deficient mice (SCID)] mice were obtained from CLEA Japan. All mice were maintained in filter-topped cages on autoclaved food and water at the University of Hokkaido and the Institute for Adult Diseases, Asahi Life Foundation, according to National Institutes of Health (NIH) guidelines. All experimental protocols were approved by the ethics committee for animal experimentation at Hokkaido University and Asahi Life Foundation. Orthotopic implantation of KYN2 cells and KYN2 transfectants were performed as described previously (30). Briefly, mice were inoculated orthotopically with 5×10^6 HSF1 control ($n = 12$) and HSF1 KD ($n = 12$) cells in 100 μl of phosphate-buffered saline, injected into the liver. Mice were killed 6 weeks after inoculation and autopsies were performed immediately. In the lipopolysaccharide (LPS)/D-galactosamine (GalN)-induced liver injury model, mice were injected intraperitoneally with LPS (20 lg/kg; Sigma) and GalN (1000 mg/kg; Wako, Osaka, Japan) (24).

Patients and tissue samples

For immunohistochemical analysis, a total of 226 adult patients with HCC who underwent curative resection between 1997 and 2006 at Hokkaido University Hospital were enrolled in this study. A preoperative clinical diagnosis of HCC was required to meet the diagnostic criteria of the American Association for the Study of Liver Diseases. Briefly, inclusion criteria were as follows: (i) distinctive pathological diagnosis, (ii) no preoperative anticancer treatment or distant metastases, (iii) curative liver resection (exclusion of extrahepatic tumor spread/metastasis) and (iv) complete clinicopathological and follow-up data. The study protocols were approved by the institutional review board and performed in compliance with the Helsinki of Declaration. Written informed consent was obtained from as many of the patients who were alive as possible (deceased cases were approved for use without written informed consent). Histological diagnosis was made according to World Health Organization criteria. The main clinicopathological features are presented in Table I. During follow-up, clinical evaluations and biochemical tests were performed every 1–3 months. Patients underwent triphasic computed tomography of the liver every 2–3 months.

Statistical analysis

Data are expressed as mean ± standard error of the mean (SEM). Significant differences were detected using non-parametric testing. Correlations between protein expression and clinicopathological features of the specimens were assessed, and the resulting data were analyzed using the χ^2 test and Fisher's exact test. Cumulative survival rate was calculated from the first date of treatment using the Kaplan–Meier life-table method. Differences were evaluated by log-rank testing. Independent factors for survival were assessed with the Cox proportional hazard regression model. Differences between the two groups were analyzed using the log-rank test. Statistical analyses were performed using Stat View software (version 5.0; SAS Institute, Cary, NC). Values of $P < 0.05$ were considered significant.

Results

Effect of HSF1 on tumor growth

We first investigated expression of HSF1 in cultured HCC cell lines. HSF1 expression was detected in all eight HCC cell lines analyzed. KYN2 cells showed significantly higher expression of HSF1 than other cell lines (Figure 1A). To further elucidate the functional role of HSF1 in HCC, we established HSF1 KD KYN2 cells by expressing the shRNA against HSF1 or control shRNA. To evaluate the effects of HSF1 on cell growth, we measured cell numbers at several time points and found that the growth of HSF1 KD cells was significantly inhibited compared with control cells (HSF1 control) (Figure 1B). Cell cycle regulators including PCNA, cyclin D1, cdc2 and CDK4 were suppressed in HSF1 KD cells compared with HSF1 control cells (Figure 1C). These results indicate that HSF1 enhances HCC cell growth. Concordantly, HSF1 KD reduced DNA synthesis as measured by bromodeoxyuridine incorporation (Figure 1D).

To evaluate the effects of HSF1 on HCC *in vivo*, orthotopic xenografts were established by HSF1 control and HSF1 KD KYN2 cells in nude mice. Maximum primary tumor diameters and tumor volumes were significantly decreased in HSF1 KD xenografts compared with HSF1 control ones (Figure 1E), suggesting that HSF1 accelerated HCC tumor growth *in vivo*. We confirmed that the tumor of HSF1 KD cells showed significantly lower expression of HSF1 and PCNA than the tumor of HSF1 control cells (Figure 1E).

We performed gain-of-function experiments for HSF1 *in vitro*. No apparent changes in cell growth were seen with overexpression of HSF1 in HCC cell lines with low HSF1 expression (Supplementary Figure 1, available at *Carcinogenesis* Online), whereas cell growth was reduced in HSF1 KD experiments, as above. Based on these

Table I. HSF1, BAG3 expression and clinicopathological variables in HCC

Parameter	Total	HSF1		*P*	BAG3		*P*
		High	Low		High	Low	
		n = 115	*n* = 111		*n* = 112	*n* = 114	
		≥30	<30		≥25	<25	
Age (years)							
≥60	126	66	60	0.69	59	67	0.42
<60	100	49	51		53	47	
Sex							
Male	185	95	90	0.86	94	91	0.49
Female	41	20	21		18	23	
Etiology							
HBsAg(+)/HCV(−)	85	45	40	0.70	39	46	0.67
HBsAg(−)/HCV(+)	84	43	41		44	40	
HBsAg(+)/HCV(+)	6	4	2		2	4	
HBsAg(−)/HCV(−)	51	23	28		27	24	
Cirrhosis							
Presence	121	64	57	0.59	62	59	0.59
Absence	105	51	54		50	55	
Tumor size (cm)							
<5	149	67	82	0.017*	66	83	0.035*
≥5	77	48	29		46	31	
No. of tumor nodules							
Solitary	168	78	90	0.032*	79	89	0.22
Multiple (≥2)	58	37	21		33	25	
TNM stage							
I and II	139	62	77	0.017*	63	76	0.11
III and IV	87	53	34		49	38	
BCLC stage							
A	81	27	54	<0.001*	32	49	0.065
B	108	64	44		58	50	
C	37	24	13		22	15	
Differentiation							
Well	36	11	25	0.010*	10	26	0.014*
Moderate	143	74	69		75	68	
Poor	47	30	17		27	20	
Capsular formation							
Presence	184	95	89	0.73	91	93	1.0
Absence	42	20	22		21	21	
Vascular invasion							
Present	37	24	13	0.073	22	15	0.21
Absent	189	91	98		90	99	
Serum AFP level							
<20	117	53	64	0.086	52	65	0.14
≥20	109	62	47		60	49	

AFP, alpha-fetoprotein; BCLC, Barcelona Clinic Liver Cancer; HCV, hepatitis C virus; TNM, tumor node metastasis.
*Significant *P* value.

findings, we concluded that HSF1 expression is a necessary condition for cell growth, but it is not a sufficient condition. We, therefore, did not further investigate gain of function of HSF1.

Impaired EGF-mediated MEK/ERK activation in HSF1 KD cells and HSF1$^{-/-}$ hepatocytes

Activation of the MEK/ERK pathway regulates many important cellular processes in carcinogenesis. To further elucidate the function of HSF1 on tumor growth, we investigated the cascade of MAPK. In WT hepatocytes and HSF1 control cells, EGF, a potent activator of MAPK, efficiently activated EGFR, MEK1/2 and ERK1/2 (Figure 2A). In contrast, activation of EGFR, MEK1/2 or ERK1/2 was significantly decreased in HSF-knockout mice (HSF$^{-/-}$) hepatocytes and HSF1 KD cells (Figure 2A and B). Regarding protein levels of EGFR, MEK1/2 and ERK1/2, EGFR protein levels were significantly decreased in HSF1$^{-/-}$ hepatocytes and HSF1 KD compared with controls, whereas other proteins were unchanged (Figure 2A and B). This result was consistent with the previous report (31). Immunohistochemical staining revealed that HSF1 control tumor showed strong phosphorylated ERK1/2 levels, whereas almost no ERK1/2 activation was observed in HSF1 KD tumors (Figure 2C).

Role of HSF1 in TNF-α-induced apoptosis

Since tumor growth inhibition is caused mainly by increased cell death and decreased cellular proliferation, we compared numbers of apoptotic cell deaths in HSF1 control and HSF KD xenografts using the TUNEL assay. Significantly more apoptotic tumor cells were found in HSF1 KD tumors than in HSF1 control tumors (Figure 3A). Next, we examined whether HSF1 was involved in apoptosis *in vitro*. FACS analysis showed very few apoptotic cells in HSF KD or HSF control in the absence of any stimuli. In contrast, treatment with TNF-α, a potent inducer of apoptosis, caused more extensive apoptotic cell death in HSF1 KD cells (23.9%) than in HSF control cells (8.7%) (Figure 3B). Furthermore, we also confirmed increased TNF-α-induced apoptosis in HSF KD cells as determined by TUNEL assay and caspase-3 activation (Figure 3C and D). To examine whether HSF1 is required for TNF-α-induced liver apoptosis *in vivo*, we used an LPS/GalN liver injury model that depends on TNF-α-mediated apoptosis (32). At 7 h LPS/GalN

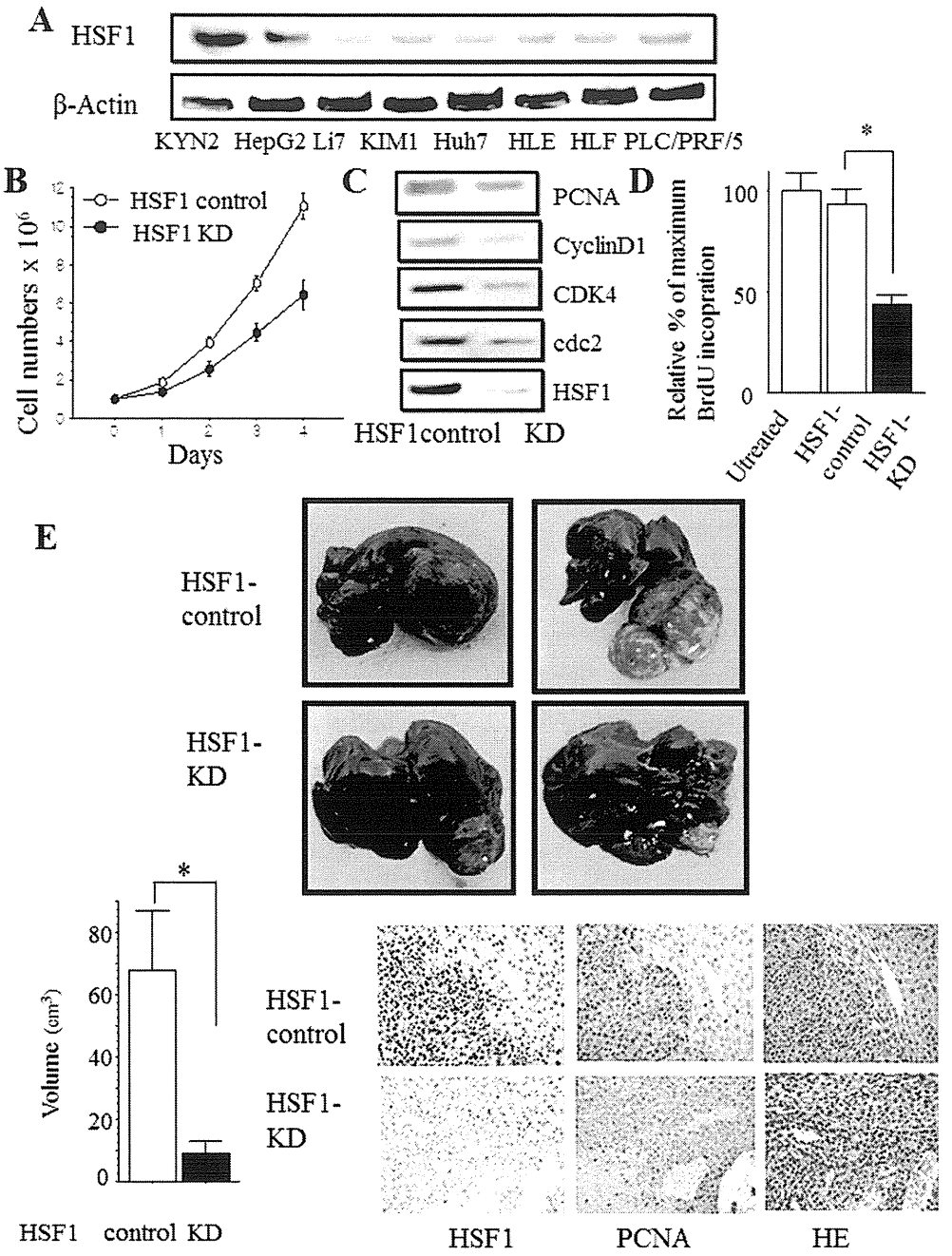

Fig. 1. Role of HSF1 in HCC growth. (**A**) Expression of HSF1 in the eight indicated HCC cell lines was determined by western blot analysis, using β-actin as a control. (**B**) Cell growth of HSF1 control KYN2 cells and HSF1 KD KYN2 cells was measured by counting the number of cells. One representative experiment from three experiments is shown. Data are plotted as mean ± SEM. (**C**) Expression of cell-cycle-related protein in HSF1 control KYN2 cells and HSF1 KD KYN2 cells, as determined by western blot analysis. (**D**) Cells were pulsed with BrdU (10 mmol/l) for 4 h. Optical density values are expressed as a percentage relative to the group expressing control. $^*P < 0.05$. Bars: SEM. (**E**) Growth appearance of HSF1 KD and HSF1 control cells in SCID mice after orthotopic implantation (upper panel). Orthotopic tumor volume was measured. Data are expressed as mean ± SEM (HSF1 control, $n = 12$; HSF1 KD, $n = 12$). $^*P < 0.05$. Bars: SEM (lower left panel). HE and immunohistochemical staining for HSF1 and PCNA (original magnification: ×40): lower right panel. BrdU, bromodeoxyuridine; HE, hematoxylin and eosin.

administration, $HSF^{-/-}$ exhibited marked alanine aminotransferase elevation (Figure 3E), severe histological liver damage and hepatocyte apoptosis compared with WT mice (Figure 3E). This was also in accordance with the notable depression of HSF1 inducing apoptosis *in vitro*.

HSF1 is involved in TNF-α-mediated NF-κB activation

Regarding the association between HSF1 and antiapoptosis, expression of bcl-2-associated athanogene domain 3 (BAG3) was reportedly reduced in HSF1 KD cells compared with control cells (7,11). In addition, microarray array analysis showed that BAG3 was dramatically downregulated in HSF1 KD cells compared with HSF1 control cells (Supplementary Table I, available at *Carcinogenesis* Online). Immunoblot analysis showed that BAG3 protein expression was reduced in $HSF1^{-/-}$ hepatocytes and HSF1 KD cells relative to the respective controls (Figure 4A and B). Meanwhile, activation of IKK and NF-κB pathway represents one of the most important antiapoptotic signals. In addition, BAG3 is also reported to control proteasomal degradation of IKKγ, the regulatory subunit (also called NF-κB essential modulator) of the IKK complex, and

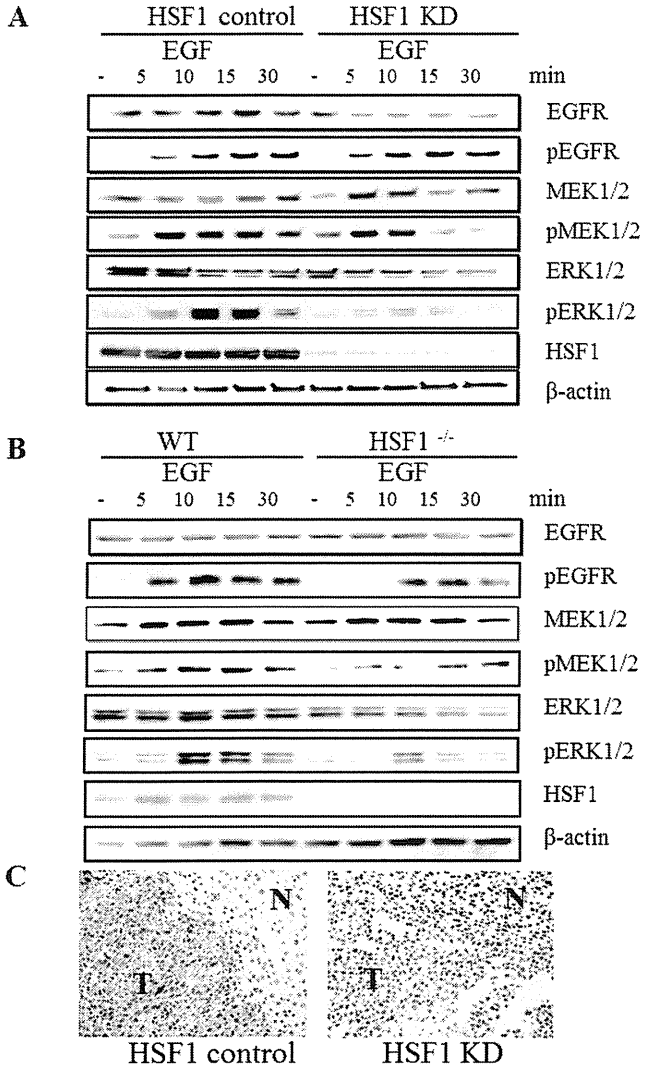

Fig. 2. EGF-mediated MEK/ERK activation is impaired in HSF1 KD cells and HSF1$^{-/-}$ hepatocytes. (**A**) HSF1 control and KD cells were treated with EGF (10 ng/ml), lysed at the indicated times, gel separated and immunoblotted with antibodies against indicated proteins. (**B**) HSF1 WT and HSF$^{-/-}$ hepatocytes were treated with TNF-α (30 ng/ml), lysed in indicated times, gel separated and immunoblotted with antibodies against indicated proteins. (**C**) Representative phosphorylated ERK (p-ERK) staining of orthotopic tumors of HSF1 control and KD cells (original magnification: ×40). N, non-cancerous liver; T, tumor.

NF-κB activity (33). Regarding the NF-κB pathway, NF-κB activation by TNF-α was decreased in HSF1 KD cells compared with the control cells (Figure 4A). In contrast, without any treatment, basal NF-κB activity was very weak and no differences were apparent between HSF1 control cells and HSF1 KD cells (Figure 4A). Consistent with this, microarray analysis showed no apparent differences in the expression of typical NF-κB-regulated genes. We also performed NF-κB pathway analysis and found that the pathway was not overrepresented by the microarray results (Supplementary Figure 2, available at *Carcinogenesis* Online). Next, we investigated whether HSF1 is involved in TNF-α-mediated NF-κB activation and found that phosphorylated Iκk-B (p-IκB), a marker of NF-κB activation, was significantly decreased in HSF$^{-/-}$ hepatocytes and HSF1 KD cells compared with their controls. As expected, IKKγ protein levels were dramatically reduced in HSF1$^{-/-}$ hepatocytes and HSF1 KD cells compared with their controls (Figure 4A and B). To investigate whether decreased IKKγ protein was degraded via proteasome, we used the proteasomal inhibitor, MG-132, and found that protein levels of IKKγ in HSF1 KD cells recovered with the inhibitor, whereas protein expression of BAG3 was unchanged (Figure 4C). Although mRNA levels of BAG3 were significantly downregulated in HSF1 KD cells compared with HSF1 control cells, mRNA levels of IKKγ were not changed (Figure 4D). HSP70 mRNA and protein levels were similar between HSF1 control and HSF1 KD cells (Figure 4A–D). These results suggest that HSF1 positively regulated BAG3 expression, which stabilized the IKKγ protein necessary for NF-κB activation. Immunohistochemical staining revealed that downregulation of HSF1 dramatically reduced BAG3 levels in HSF1 KD xenografts compared with the HSF1 control xenografts.

We performed real-time PCR analysis of the putative NF-κB-regulated antiapoptotic genes. The levels of A20, cellular inhibitor of apoptosis 2 (c-IAP2) RNA expression were decreased in HSF1 KD cells by TNF-α-mediated compared with HSF1 control cells, whereas cylindromatosis, cIAP1 were unchanged (Figure 4E). These results suggest that HSF1 plays an important role in tumor growth via MAPK-mediated cellular proliferation and NF-κB-mediated antiapoptosis.

HSF1 and BAG3 were frequently overexpressed in human HCCs

To analyze the involvement of HSF1 in HCCs, we examined expression levels of HSF1 in human primary HCCs. Immunoblot analysis showed that levels of HSF1 in HCC tissues were significantly higher than in non-cancerous liver tissues in 5 of 10 samples (50%) (Figure 5A). We tested 226 samples from tumor tissues of patients with HCCs by immunohistochemistry. The median percentage of positive cells was 30% (range: 0–90.0%) and we divided patients into two groups of high expressers and low expressers based on the percentage of HSF1-positive cells using a cutoff level of 30%, representing the median value of HSF1. We found that 50.9% (115/226) of tumor samples showed high HSF1 expression. Typical examples of high HSF1 expression samples are shown in Figure 5B. The characteristics of patients in this analysis are shown in Table I. Significant differences were apparent between high and low HSF1 expression groups in terms of tumor size ($P = 0.017$), tumor node metastasis stage ($P = 0.017$), Barcelona Clinic Liver Cancer stage ($P < 0.001$), number of tumor nodules ($P = 0.032$) and histological grade ($P = 0.010$) (Table I), but no significant correlations were observed between HSF1 expression and other clinicopathological variables such as etiology or cirrhosis (Table I). Furthermore, patients with tumors showing HSF1 overexpression displayed significantly shorter overall survival (median: 75.2 months) compared with patients whose tumors showed HSF1 low expression (median: 136.0 months; $P = 0.004$, log-rank test) (Figure 5C). These findings suggest that overexpression of HSF1 was frequently observed in human HCCs, particularly in tumors exhibiting aggressive features.

To explore the pathological relationship between HSF1 and BAG3 in HCC samples, we performed immunohistochemical analysis for BAG3 in 226 HCC samples, which were also analyzed for HSF1 immunohistochemistry. The median percentage of positive cells was 25% (range: 0–85.0%) and we divided them into two groups—high expressers and low expressers—based on the percentage of BAG3-positive cells using a cutoff level of 25%, representing the median value of BAG3. Representative examples of immunohistochemical reactivity for BAG3 are shown in Figure 5B. Expressions of BAG3 protein were significantly increased in HCC specimens, whereas no or only low BAG3 expression was seen in adjacent non-cancerous tissue. BAG3 expression correlated significantly with histological grade ($P = 0.014$), and tumor size ($P = 0.035$), but no significant correlations were observed between BAG3 expression and other clinicopathological variables (Table I). Furthermore, a positive correlation between expressions of HSF1 and BAG3 was found in HCC ($P < 0.05$; Figure 5D) and patients with tumors showing BAG3 overexpression displayed significantly shorter overall survival (median: 84.0 months) compared with those patients whose tumors showed BAG3 low expression (median: 134.2 months; $P = 0.015$, log-rank test) (Figure 5E). Multivariate Cox regression

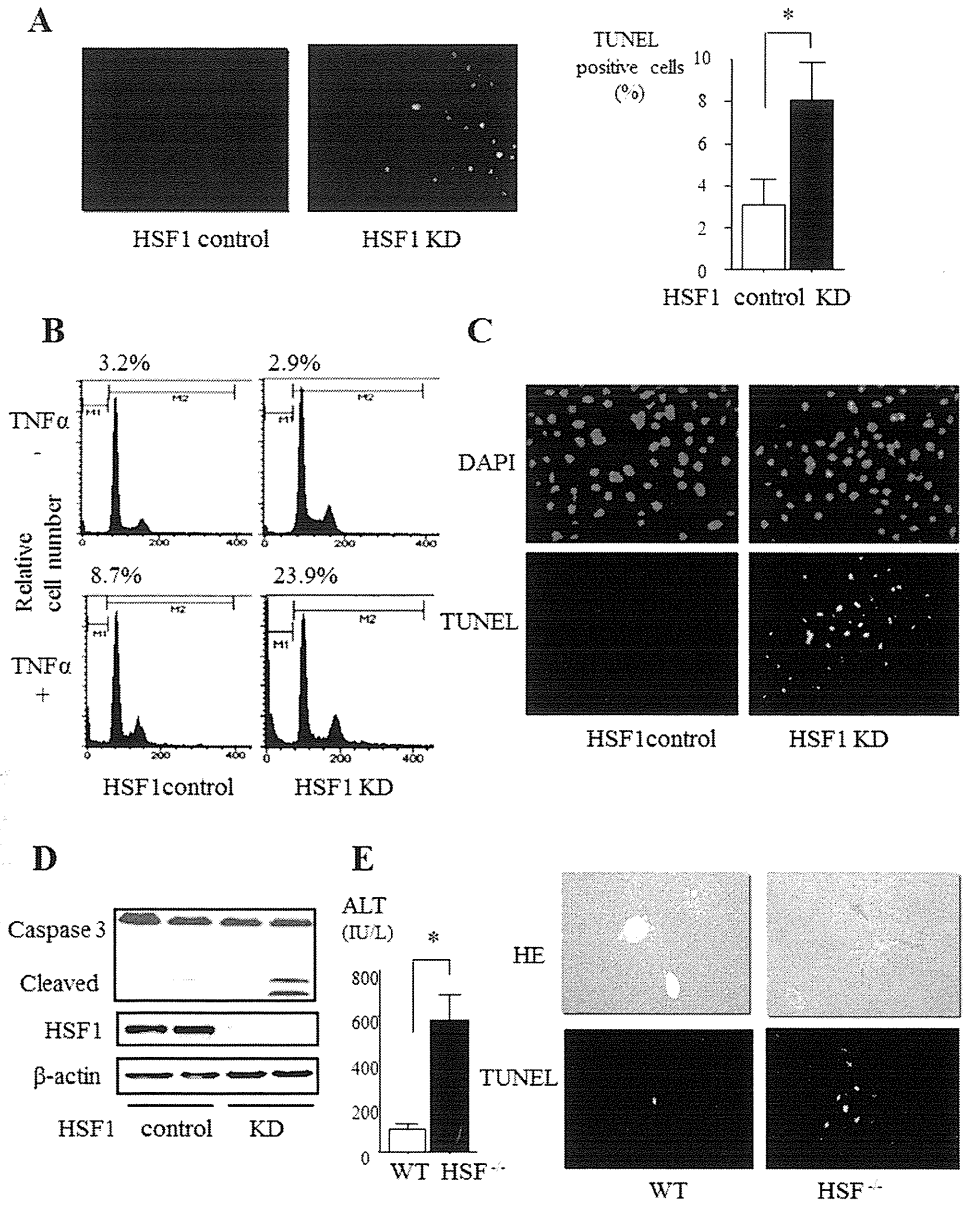

Fig. 3. Antiapoptotic effect of HSF1 in HCC cells and hepatocytes. (**A**) TUNEL staining was performed in tumors of HSF1 control and HSF1 KD cells from orthotopic implanted mice (left panel). TUNEL-positive cells were counted in tumors of HSF1 control and HSF1 KD cells. *$P < 0.05$. Bars: SEM (right panel). (**B**) Apoptotic cells were evaluated by FACS at 24 h after incubation with TNF-α (30 ng/ml). Values indicate percentages of cells with sub-G_1 DNA content. Representative data are shown from three independent experiments. (**C**) TUNEL staining was performed in HSF1 control and KD cells after incubation with TNF-α. (**D**) Protein expressions of caspase 3, HSF1 and β-actin in TNF-α-treated HSF1 control and KD cells were determined by western blot analysis. (**E**) Serum ALT levels 7 h after injection of WT and $HSF1^{-/-}$ mice with LPS (5 μg/kg) and GalN (500 mg/kg). *$P < 0.05$, compared with WT mice (left panel). HE and TUNEL stainings were performed in sections of livers obtained 7 h after injecting LPS (5 μg/kg) and GalN (500 mg/kg) into WT and $HSF1^{-/-}$ mice (right panel). ALT, alanine aminotransferase; DAPI, 4′,6-diamidino-2-phenylindole; HE, hematoxylin and eosin.

analysis identified high HSF1 expression (hazard ratio: 2.07; $P = 0.04$) as an independent prognostic factor for overall survival (Table II).

Discussion

As a master regulator of the heat shock response, HSF1 enhances organism survival and longevity in the face of environmental challenges. However, HSF1 can also act to the detriment of organisms by supporting malignant transformation (34). As reported previously, loss of HSF1 negatively impacts tumorigenesis driven by p53 or Ras mutations (8,16). Since HSF1 does not act as a classic oncogene, the increased resistance to proteotoxic stress induced by HSF1 was suggested to support tumor initiation and growth by enabling cells to accommodate the genetic alterations that accumulate during malignancy (35). However, the specific mechanisms by which HSF1 may support the growth of tumors are not well understood. Here, we have demonstrated that HSF1 has detrimental effects on liver tumor growth. We also proposed that the antiapoptotic effect of HSF1 may play a role in HCC tumor growth.

To clarify the mechanisms underlying this effect, we investigated associations between HSF1 and the NF-κB signaling pathway. Although, in a previous study, heat shock blocked the degradation of IκB (36) and nuclear translocation of NF-κB, the recent literature has reported that the presence of constitutively active HSF1 does not block TNF-α-induced activation of the NF-κB pathway or expression of a set of NF-κB-dependent genes (37). The current study established HSF1 KD cells and showed that HSF1 was necessary for TNF-α-induced NF-κB activation. We analyzed the function of BAG3 as a candidate for the molecule connecting HSF1 with NF-κB activation. BAG3 has reportedly been characterized by the

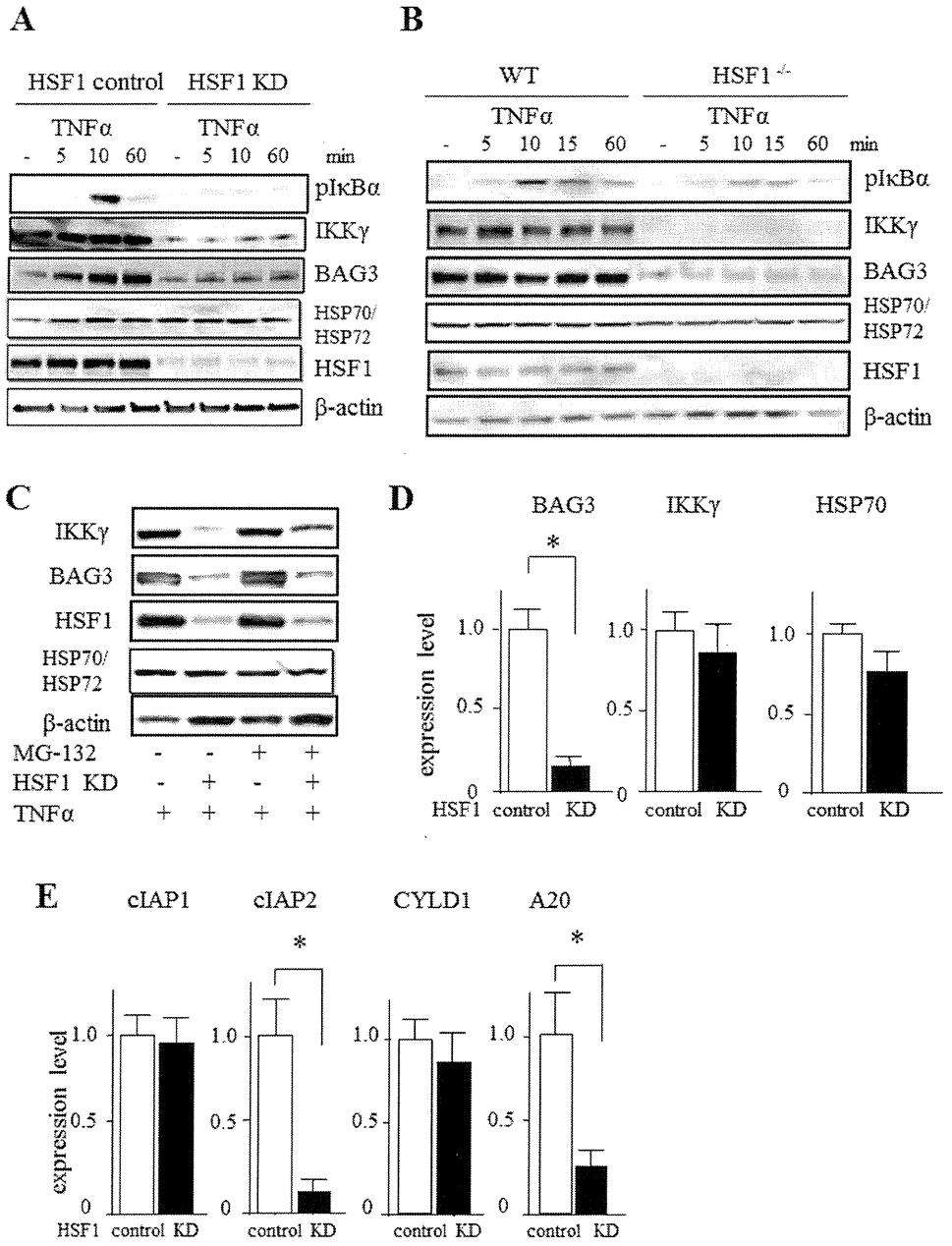

Fig. 4. HSF1 is involved in TNF-α-mediated NF-κB activation. (**A**) HSF1 control and KD cells were treated with TNF-α (30 ng/ml), lysed at the indicated times, gel separated and immunoblotted with antibodies against the indicated proteins. (**B**) HSF1 WT and HSF$^{-/-}$ hepatocytes treated with TNF-α (30 ng/ml), lysed at the indicated times, gel separated and immunoblotted with antibodies against the indicated proteins. (**C**) HSF1 control and KD cells were treated with TNF-α (30 ng/ml) with or without MG-132, lysed at 24 h, gel separated and immunoblotted with antibodies against indicated proteins. (**D**) Relative mRNA levels for BAG3, IKKγ and HSP70 in HSF1 control and KD cells determined by real-time PCR. Data are expressed as mean ± SEM ($n = 4$ per group). *$P < 0.05$. Bars: SEM. (**E**) Relative mRNA levels for antiapoptosis-related gene in HSF1 control and KD cells as determined by real-time PCR. Data are expressed as mean ± SEM ($n = 4$ per group). *$P < 0.05$. Bars: SEM. CYLD, cylindromatosis.

interaction with a variety of partners (Raf-1, steroid hormone receptors and HSP70) and is involved in regulating a number of cellular processes, particularly those associated with antiapoptosis (38). This molecule was expressed in response to stressful stimuli in a number of normal cell types and appears constitutively in a variety of tumors (33,39), and gene expression is regulated by HSF1 (40). In addition, knockdown of BAG3 protein decreased IKKγ levels, increasing tumor cell apoptosis and inhibiting tumor growth (33). Based on these considerations, we investigated whether attenuating HSF1 would enhance IKKγ protein expression, and data with MG-132 show that proteasomal degradation of IKKγ is enhanced in HSF1 KD cells. In addition, knowledge of the role BAG3 plays in preventing the proteasomal turnover of certain proteins suggests that the loss of BAG3 in HSF1 KD cells may be responsible for the enhanced turnover of IKKγ in this setting.

NF-κB activation is a master regulatory step in antiapoptosis. Several mechanisms have been reported regarding this antiapoptotic effect of NF-κB activation (41). NF-κB exerts its prosurvival activity primarily through the induction of target genes, the products of which inhibit components of the apoptotic machinery. These include Bcl-X_L and c-IAP (41), which binds directly to and inhibits the effect of caspases. This study showed that inactivation of NF-κB promoted apoptotic effects against TNF-α in HSF1$^{-/-}$ hepatocytes and HSF1 KD HCC cells. Real-time PCR analyses indicated that expression levels of apoptosis-related genes such as A20 and c-IAP2 were decreased by inhibition of NF-κB activation, whereas apoptosis-related genes such

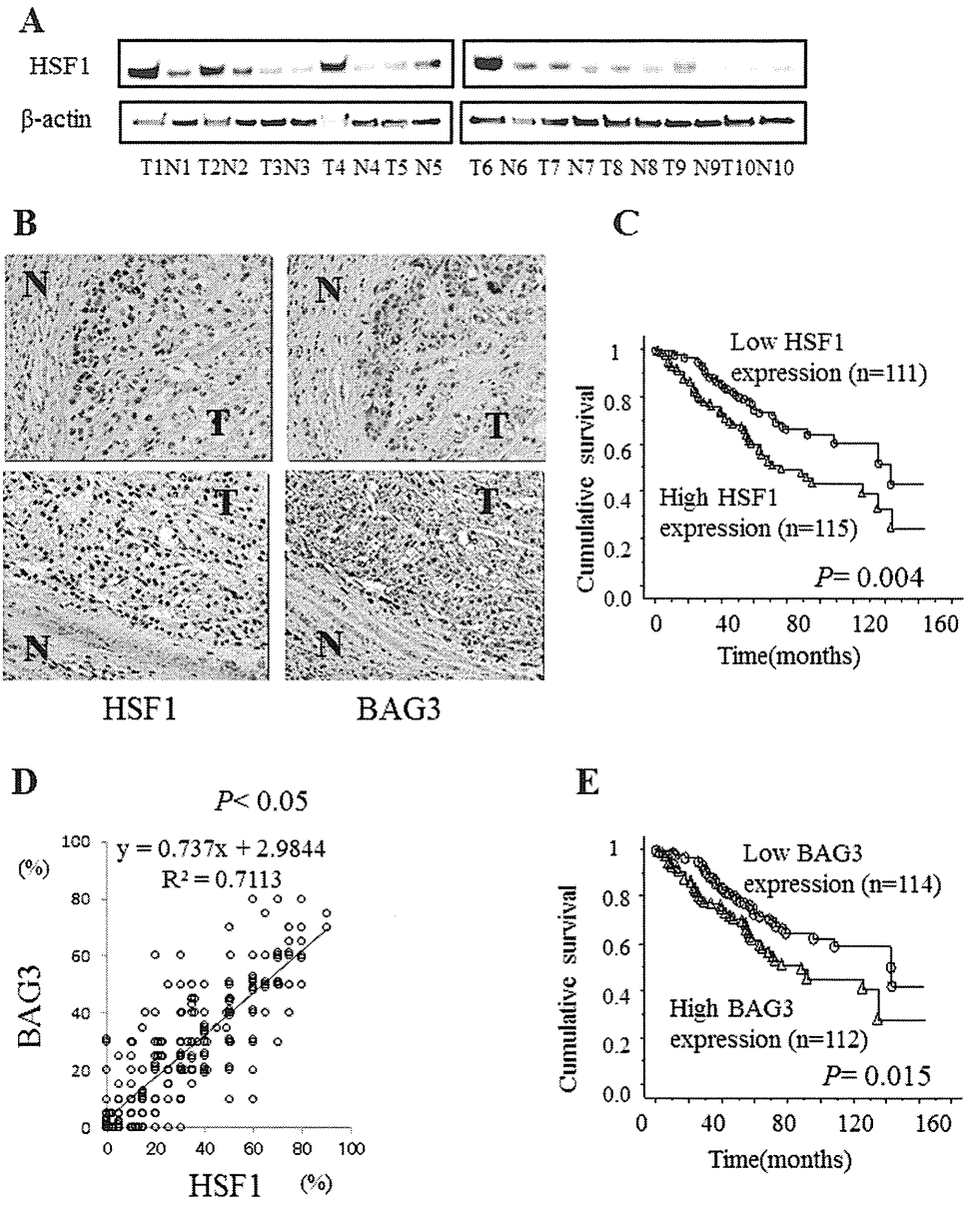

Fig. 5. Overexpression of HSF1 protein in human HCCs and pathological relationship between HSF1 and BAG3 in HCC samples. (**A**) HSF1 protein expression was determined in paired samples of human non-neoplastic liver and HCC by western blot, using β-actin as a control. N, non-cancerous liver; T, tumor. (**B**) Representative HSF1 and BAG3 staining of HCC and surrounding tissue. (**C**) Correlation of HSF1 overexpression with overall survival rates of patients. (**D**) Relationship between BAG3 and HSF1 expression in HCC. Scatterplot of BAG3 versus HSF1 with regression line displaying a correlation according to Spearman's correlation coefficient ($P < 0.01$). (**E**) Correlation of BAG3 overexpression with overall survival rates of patients.

as cIAP1 and cylindromatosis, which are known to be regulated by NF-κB activation, were apparently unaffected. Whether gene expression regulated by NF-κB activity differs between inducible and basal activation remains to be determined.

Regarding the relationship between HSF1 and HCC development, HSF1-deficient mice recently revealed dramatically reduced numbers and sizes of tumors compared with WT controls when tumors were induced by the chemical carcinogen, diethylnitrosamine. The same study suggested that the presence of extensive pathology associated with severe steatosis by diethylnitrosamine was prevented by HSF1 deletion and may be associated with reduced HCC development (42). On the other hand, ablation of IKKγ in liver parenchymal cells caused spontaneous development of HCC in mice, with tumor development preceded by steatohepatitis (43). Based on these observations, we assume that reductions in diethylnitrosamine-induced HCC development among HSF1-deficient mice may be associated with reduced expression of IKKγ, the reduction of which caused the steatosis.

BAG3 is a critical regulator of apoptosis in HSF1-deficient hepatocytes and HSF1 KD HCC cells. Moreover, the relationship between HSF1 and BAG3 has been shown not only in cell cultures and mouse models, but also in human HCC tissue samples; a correlation between HSF1 expression and BAG3 expression was found in HCC. Clinicopathological features and biological results provide a mechanistic link between HSF1 and HCC development via BAG3.

As for the ERK signal, a previous study demonstrated that impairment of JNK and ERK signaling in HSF1$^{-/-}$ MEF cells was caused in part by the reduced expression of EGFR (33). We showed a slight decrease in expression of EGFR among HSF1-deficient hepatocytes and HSF1 KD cells. On the other hand, the level of reduced activation of ERK, as a downstream molecule of EGFR, was larger than expected. However, the detailed mechanisms by which HSF1 regulates MAPK need further investigation.

In conclusion, we found that HSF1 deficiency significantly diminished NF-κB and MAPK activation in HCC hepatocytes and

Table II. Multivariate analysis with a Cox proportional hazards regression model

Characteristic	Univariate analysis	Multivariate analysis	Hazard ratio (95% CI)
Age (≥60 years)	0.22	0.15	
Gender (male)	0.92	0.53	
HCV status (positive)	0.28	0.82	
Cirrhosis (positive)	0.15	0.066	
Tumor size (≥50 mm)	<0.01*	0.011*	2.21 (1.18–4.12)
No. of tumor nodule (multiple)	<0.01*	<0.01*	2.67 (1.38–5.62)
Tumor differentiation (poor)	<0.01*	0.031*	2.34 (1.33–4.11)
Capsular formation (absence)	0.18	0.36	
Vascular invasion (presence)	0.062	0.10	
TNM stage (III + IV versus I + II)	<0.01*	0.020*	2.35 (1.14–4.82)
AFP (≥20 ng/ml)	0.18	0.36	
HSF1 expression (high)	0.018*	0.040*	2.07 (1.22–3.50)
BAG3 expression (high)	0.043*	0.056	

AFP, alpha-fetoprotein; CI, confidence interval; HCV, hepatitis C virus; TNM, tumor node metastasis.
*Significant *P* value.

HCC cells; accordingly, HSF1 deficiency inhibited the development of HCC. Furthermore, clinicopathological analysis demonstrated a significant correlation between HSF1 or BAG3 protein levels and prognosis. Our results demonstrate the importance of HSF1 in human HCCs and suggest inhibition of HSF1 as a novel strategy to target that subset of HCC patients in whom this protein is overexpressed.

Supplementary material

Supplementary Materials and methods, Table I and Figures 1 and 2 can be found at http://carcin.oxfordjournals.org/

Funding

Ministry of Education, Culture, Sports, Science and Technology, Japan (to N.S.); Japan Society for the Promotion of Science (24390185, 24659359); Ministry of Health, Labour and Welfare Japan; Japan Health Sciences Foundation; grants-in-aid for scientific research (22300317) and Uehara Memorial Foundation (to S.M.).

Conflict of Interest Statement: None declared.

References

1. El-Serag,H.B. (2012) Epidemiology of viral hepatitis and hepatocellular carcinoma. *Gastroenterology*, **142**, 1264–1273.e1.
2. Cheng,A.L. *et al.* (2009) Efficacy and safety of sorafenib in patients in the Asia-Pacific region with advanced hepatocellular carcinoma: a phase III randomised, double-blind, placebo-controlled trial. *Lancet Oncol.*, **10**, 25–34.
3. Breuhahn,K. *et al.* (2011) Strategies for hepatocellular carcinoma therapy and diagnostics: lessons learned from high throughput and profiling approaches. *Hepatology*, **53**, 2112–2121.
4. Pirkkala,L. *et al.* (2001) Roles of the heat shock transcription factors in regulation of the heat shock response and beyond. *FASEB J.*, **15**, 1118–1131.
5. Sorger,P.K. (1991) Heat shock factor and the heat shock response. *Cell*, **65**, 363–366.
6. Guertin,M.J. *et al.* (2010) Chromatin landscape dictates HSF binding to target DNA elements. *PLoS Genet.*, **6**, e1001114.
7. Mendillo,M.L. *et al.* (2012) HSF1 drives a transcriptional program distinct from heat shock to support highly malignant human cancers. *Cell*, **150**, 549–562.
8. Page,T.J. *et al.* (2006) Genome-wide analysis of human HSF1 signaling reveals a transcriptional program linked to cellular adaptation and survival. *Mol. Biosyst.*, **2**, 627–639.
9. Dai,C. *et al.* (2007) Heat shock factor 1 is a powerful multifaceted modifier of carcinogenesis. *Cell*, **130**, 1005–1018.
10. Hayashida,N. *et al.* (2006) A novel HSF1-mediated death pathway that is suppressed by heat shock proteins. *EMBO J.*, **25**, 4773–4783.
11. Jacobs,A.T. *et al.* (2007) Heat shock factor 1 attenuates 4-hydroxynonenal-mediated apoptosis: critical role for heat shock protein 70 induction and stabilization of Bcl-XL. *J. Biol. Chem.*, **282**, 33412–33420.
12. Vydra,N. *et al.* (2006) Spermatocyte-specific expression of constitutively active heat shock factor 1 induces HSP70i-resistant apoptosis in male germ cells. *Cell Death Differ.*, **13**, 212–222.
13. Neckers,L. *et al.* (2012) Hsp90 molecular chaperone inhibitors: are we there yet? *Clin. Cancer Res.*, **18**, 64–76.
14. Khalil,A.A. *et al.* (2011) Heat shock proteins in oncology: diagnostic biomarkers or therapeutic targets? *Biochim. Biophys. Acta*, **1816**, 89–104.
15. Chuma,M. *et al.* (2003) Expression profiling in multistage hepatocarcinogenesis: identification of HSP70 as a molecular marker of early hepatocellular carcinoma. *Hepatology*, **37**, 198–207.
16. Cai,L. *et al.* (2003) The tumor-selective over-expression of the human Hsp70 gene is attributed to the aberrant controls at both initiation and elongation levels of transcription. *Cell Res.*, **13**, 93–109.
17. Min,J.N. *et al.* (2007) Selective suppression of lymphomas by functional loss of Hsf1 in a p53-deficient mouse model for spontaneous tumors. *Oncogene*, **26**, 5086–5097.
18. Santagata,S. *et al.* (2011) High levels of nuclear heat-shock factor 1 (HSF1) are associated with poor prognosis in breast cancer. *Proc. Natl Acad. Sci. USA*, **108**, 18378–18383.
19. Dudeja,V. *et al.* (2011) Prosurvival role of heat shock factor 1 in the pathogenesis of pancreatobiliary tumors. *Am. J. Physiol. Gastrointest. Liver Physiol.*, **300**, G948–G955.
20. Hoang,A.T. *et al.* (2000) A novel association between the human heat shock transcription factor 1 (HSF1) and prostate adenocarcinoma. *Am. J. Pathol.*, **156**, 857–864.
21. Ishiwata,J. *et al.* (2012) State of heat shock factor 1 expression as a putative diagnostic marker for oral squamous cell carcinoma. *Int. J. Oncol.*, **40**, 47–52.
22. Kojiro,M. *et al.* (2009) Pathologic diagnosis of early hepatocellular carcinoma: a report of the international consensus group for hepatocellular neoplasia. *Hepatology*, **49**, 658–664.
23. Fabregat,I. *et al.* (2007) Survival and apoptosis: a dysregulated balance in liver cancer. *Liver Int.*, **27**, 155–162.
24. Nakagawa,H. *et al.* (2011) Apoptosis signal-regulating kinase 1 inhibits hepatocarcinogenesis by controlling the tumor-suppressing function of stress-activated mitogen-activated protein kinase. *Hepatology*, **54**, 185–195.
25. Sun,B. *et al.* (2008) NF-kappaB signaling, liver disease and hepatoprotective agents. *Oncogene*, **27**, 6228–6244.
26. Maeda,S. *et al.* (2005) IKKbeta couples hepatocyte death to cytokine-driven compensatory proliferation that promotes chemical hepatocarcinogenesis. *Cell*, **121**, 977–990.
27. Beeram,M. *et al.* (2005) Raf: a strategic target for therapeutic development against cancer. *J. Clin. Oncol.*, **23**, 6771–6790.
28. Whittaker,S. *et al.* (2010) The role of signaling pathways in the development and treatment of hepatocellular carcinoma. *Oncogene*, **29**, 4989–5005.
29. Inouye,S. *et al.* (2003) Activation of heat shock genes is not necessary for protection by heat shock transcription factor 1 against cell death due to a single exposure to high temperatures. *Mol. Cell. Biol.*, **23**, 5882–5895.
30. Chuma,M. *et al.* (2004) Overexpression of cortactin is involved in motility and metastasis of hepatocellular carcinoma. *J. Hepatol.*, **41**, 629–636.
31. O'Callaghan-Sunol,C. *et al.* (2006) Heat shock transcription factor (HSF1) plays a critical role in cell migration via maintaining MAP kinase signaling. *Cell Cycle*, **5**, 1431–1437.

32. Nowak,M. *et al.* (2000) LPS-induced liver injury in D-galactosamine-sensitized mice requires secreted TNF-alpha and the TNF-p55 receptor. *Am. J. Physiol. Regul. Integr. Comp. Physiol.*, **278**, R1202–R1209.
33. Ammirante,M. *et al.* (2010) IKK{gamma} protein is a target of BAG3 regulatory activity in human tumor growth. *Proc. Natl Acad. Sci. USA*, **107**, 7497–7502.
34. Meng,L. *et al.* (2010) Heat-shock transcription factor HSF1 has a critical role in human epidermal growth factor receptor-2-induced cellular transformation and tumorigenesis. *Oncogene*, **29**, 5204–5213.
35. Solimini,N.L. *et al.* (2007) Non-oncogene addiction and the stress phenotype of cancer cells. *Cell*, **130**, 986–988.
36. Malhotra,V. *et al.* (2002) Heat shock inhibits activation of NF-kappaB in the absence of heat shock factor-1. *Biochem. Biophys. Res. Commun.*, **291**, 453–457.
37. Janus,P. *et al.* (2011) NF-κB signaling pathway is inhibited by heat shock independently of active transcription factor HSF1 and increased levels of inducible heat shock proteins. *Genes Cells*, **16**, 1168–1175.
38. Rosati,A. *et al.* (2011) BAG3: a multifaceted protein that regulates major cell pathways. *Cell Death Dis.*, **2**, e141.
39. Homma,S. *et al.* (2006) BAG3 deficiency results in fulminant myopathy and early lethality. *Am. J. Pathol.*, **169**, 761–773.
40. Franceschelli,S. *et al.* (2008) Bag3 gene expression is regulated by heat shock factor 1. *J. Cell. Physiol.*, **215**, 575–577.
41. Luo,J.L. *et al.* (2005) IKK/NF-kappaB signaling: balancing life and death–a new approach to cancer therapy. *J. Clin. Invest.*, **115**, 2625–2632.
42. Jin,X. *et al.* (2011) Heat shock transcription factor 1 is a key determinant of HCC development by regulating hepatic steatosis and metabolic syndrome. *Cell Metab.*, **14**, 91–103.
43. Luedde,T. *et al.* (2007) Deletion of NEMO/IKKgamma in liver parenchymal cells causes steatohepatitis and hepatocellular carcinoma. *Cancer Cell*, **11**, 119–132.

Received December 4, 2012; revised August 22, 2013; accepted August 28, 2013

PLOS ONE

Critical Role of Interferon-α Constitutively Produced in Human Hepatocytes in Response to RNA Virus Infection

Yoji Tsugawa[1,2], Hiroki Kato[3], Takashi Fujita[3], Kunitada Shimotohno[4], Makoto Hijikata[1,2]*

1 Laboratory of Human Tumor Viruses, Institute for Virus Research, Kyoto University, Kyoto, Japan, **2** Laboratory of Viral Oncology, Graduate School of Biostudies, Kyoto University, Kyoto, Japan, **3** Laboratory of Molecular Genetics, Institute for Virus Research, Kyoto University, Kyoto, Japan, **4** The Research Center for Hepatitis and Immunology, National Center for Global Health and Medicine, Ichikawa, Japan

Abstract

Several viruses are known to infect human liver and cause the hepatitis, but the interferon (IFN) response, a first-line defense against viral infection, of virus-infected hepatocytes is not clearly defined yet. We investigated innate immune system against RNA viral infection in immortalized human hepatocytes (HuS-E/2 cells), as the cells showed similar early innate immune responses to primary human hepatocytes (PHH). The low-level constitutive expression of IFN-α1 gene, but not IFN-β and IFN-λ, was observed in both PHH and HuS-E/2 cells in the absence of viral infection, suggesting a particular subtype(s) of IFN-α is constitutively produced in human hepatocytes. To examine the functional role of such IFN-α in the antiviral response, the expression profiles of innate immune-related genes were studied in the cells with the treatment of neutralization against type I IFN receptor 2 (IFNAR2) or IFN-α itself to inhibit the constitutive IFN-α signaling before and after virus infection. As the results, a clear reduction of basal level expression of IFN-inducible genes was observed in uninfected cells. When the effect of the inhibition on the cells infected with hepatitis C virus (HCV) was examined, the significant decrease of IFN stimulated gene expression and the enhancement of initial HCV replication were observed, suggesting that the steady-state production of IFN-α plays a role in amplification of antiviral responses to control the spread of RNA viral infection in human hepatocytes.

Citation: Tsugawa Y, Kato H, Fujita T, Shimotohno K, Hijikata M (2014) Critical Role of Interferon-α Constitutively Produced in Human Hepatocytes in Response to RNA Virus Infection. PLoS ONE 9(2): e89869. doi:10.1371/journal.pone.0089869

Editor: Hak Hotta, Kobe University, Japan

Received September 25, 2013; **Accepted** January 24, 2014; **Published** February 26, 2014

Funding: This work was supported by grants-in-aid from the Ministry of Health, Labour and Welfare of Japan. The funders had no role in study design, data collection and analysis, decision to publish, or preparation of the manuscript.

Competing Interests: The authors have declared that no competing interests exist.

* E-mail: mhijikat@virus.kyoto-u.ac.jp

Introduction

It has been shown that the replication of RNA viruses, including Sendai virus (SeV), Vesicular stomatitis virus, Newcastle disease virus, Sindbis virus, and Hepatitis C virus (HCV) is suppressed by type I interferon (IFN) (IFN-α and IFN-β) produced rapidly from the cells after infection of viruses [1,2]. The cytosolic RNA helicases, including retinoic acid-inducible gene (RIG)-I, have been identified as receptors of pathogen-associated molecular patterns of RNA viruses [3]. After recognition of RNA virus infection by those receptors, signal cascades for induction of IFNs are stimulated and result in the activation of IFN regulatory factor (IRF)-3, and IRF-7 which are transcription factors for induction of type I IFN genes [3,4]. IRF-3 is constitutively produced in many cell types and tissues and phosphorylated after virus infection. Phosphorylated IRF-3 forms a dimer (either a homodimer or a heterodimer with IRF-7) and is translocated to the nucleus. Unlike IRF-3, IRF-7 is constitutively produced only in small amounts, if any, but the gene expression is strongly induced by type I IFN-mediated signaling in most cell types and tissues. The produced IFNs by the way described above then are secreted from the viral infected cells and bind to their receptors, which consist of IFN α/β receptor (IFNAR1 and 2), on the surface of IFN producing and/or neighboring cells and deliver the IFN signal to those cells. The primary role of type I IFN is to limit spread of a variety of pathogens via initiation of the innate immune responses through induction of the genes encoding cytokines and antiviral proteins during the first days of infection [5]. These proteins exhibit antiviral effects both directly by inhibiting viral replication and indirectly by stimulating the adaptive immune system.

On the other hand, constitutive production of type I IFN has been detected in several cells without pathogen stimulation albeit at low level. The constitutive IFN-β has been revealed to be important in maintaining immune homeostasis and essential for immune cell priming [6]. In addition, type I IFN is also known to correlate with multiple biological activities, including anti-proliferative, anti-tumor, pro-apoptotic, and immunomodulatory functions [6,7]. Previously it was reported that the IFN-α mRNA was expressed in the human normal liver [8]. However, what cell type in the human liver is responsible for the expression and what is the biological role have not been clear yet.

Our previous data showed that immortalized human hepatocytes, HuS-E/2 cells, support the whole life cycle of blood-borne HCV (HCVbb) [9]. The infection and proliferation of HCVbb in HuS-E/2 cells were enhanced by ectopic expression of a dominant-negative form of IRF-7, but not that of IRF-3, suggesting that IRF-7, rather than IRF-3, plays a primary role in regulation of HCV proliferation in these cells [10]. IRF-7 mRNA was detected in primary hepatocytes (PHH) and HuS-E/2 cells, but not HuH-7 cells, one of hepatocellular carcinoma derived cell lines, without virus infection [10]. However, the role of

the preexisting IRF-7 and molecular mechanism of its constitutive expression in hepatocytes remains unclear, because of limited knowledge of immediate innate immune response in human hepatocytes.

As the result of study on innate immunity of human hepatocytes, here we report that active IFN-α release occurs in human hepatocytes even in the absence of virus infection. We additionally show that the constitutive IFN-α plays a critical role in the early induction of IFN genes and some IFN stimulated genes (ISGs) through the increase in expression of genes related with induction of such genes, including IRF-7 gene, before virus infection.

Materials and Methods

Cell Culture

HuH-7, Huh-7.5, HepG2, and 293FT cells were grown in Dulbecco's modified Eagle's medium (Nacalai Tesque, Kyoto, Japan) supplemented with 10% fetal bovine serum, 100 U/ml nonessential amino acids (Nacalai Tesque, Kyoto, Japan), and Antimycotic Mixed Stock Solution Penicillin 100 units/ml, Streptomycin 100 μg/ml, Amphotericin B 0.25 μg/ml (Nacalai Tesque, Kyoto, Japan). HuS-E/2 cells were cultured as previously described [10]. PHH were purchased from Gibco (Grand Island, NY, USA), the hepatocyte donor was a 58-year-old male who did not show any evidences of liver abnormalities. PHH were cultured

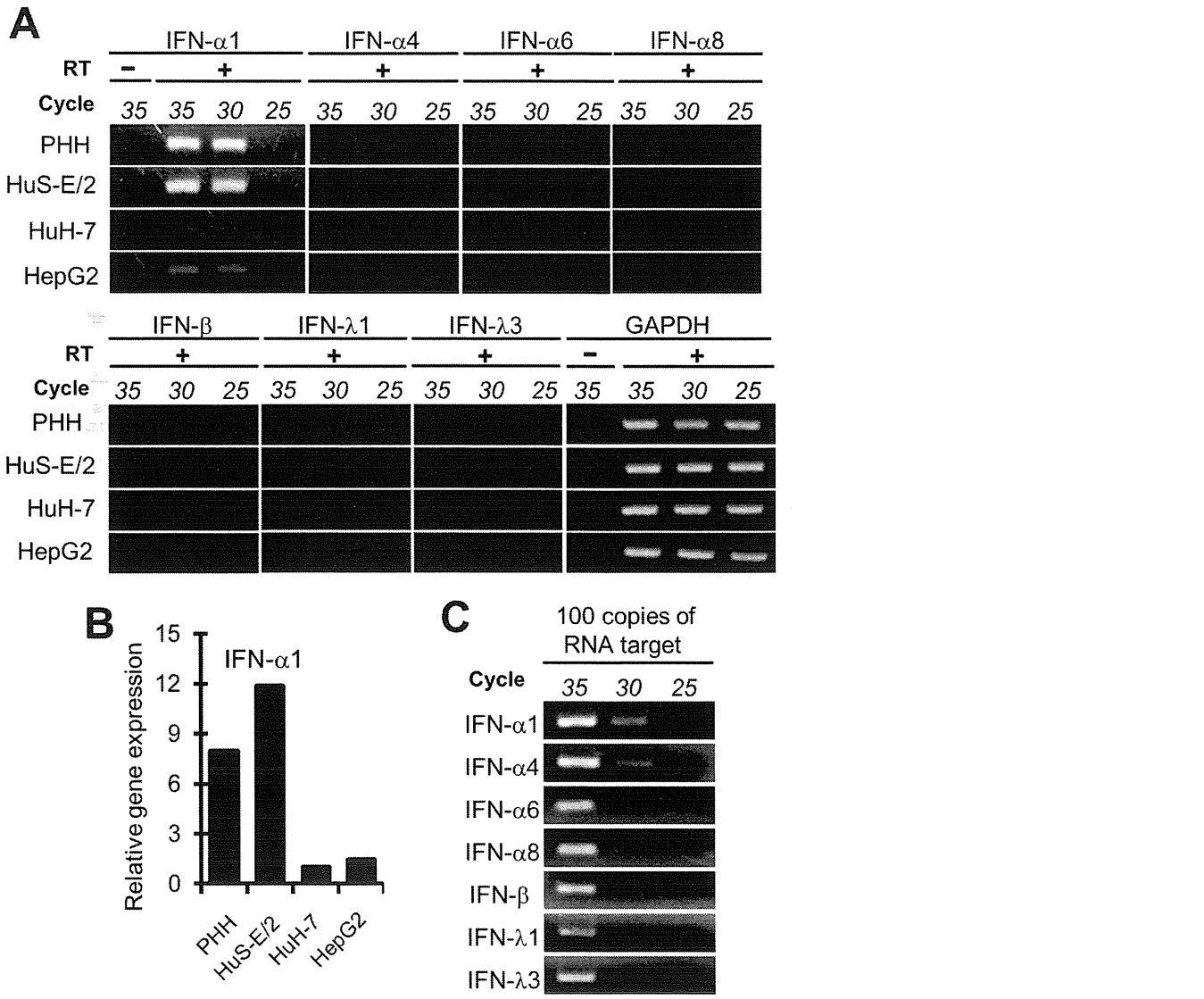

Figure 1. The expression of IFN-α1 gene in the cells derived from human hepatocytes. *A*, The expressions of several IFN genes in human hepatocyte derived cells. The presence of mRNAs for several IFN genes, IFN-α1, IFN-α4, IFN-α6, IFN-α8, IFN-β, IFN-λ1, and IFN-λ3, in PHH, HuS-E/2, HuH-7, and HepG2 cells without virus infection was examined by RT-PCR with different amplification cycles, 25, 30 and 35 cycles. RT-PCR was done with (+) or without (−) reverse transcriptase (RT) reaction. PCR products were separated in the agarose gel and stained with ethidium bromide. GAPDH mRNA was used as an internal standard substance. *B*, Semi-quantitative estimation of IFN-α1 mRNA in those cells. The relative amount of mRNA for IFN-α1 in those cells was estimated by qRT-PCR. The results of qRT-PCR were presented as relative gene expression using the RNA level of HuH-7 cells as a benchmark. *C*. Evaluation of sensitivity of RT-PCR system employed in the detection of IFN subtypes in small quantity. To show the sensitivity of RT-PCR system in this study, RT-PCR was performed with different amplification cycles, 25, 30 and 35 cycles using a primer set described in Table S1 and one hundred copies of in vitro synthesized RNA of each IFN subtype as a template.
doi:10.1371/journal.pone.0089869.g001